Journal of Solid Mechanics Vol. 16, No. 2 (2024) pp. 120-146
DOI: 10.60664/jsm.2024.0061599

Research Paper

Thermodynamics Stability of Sandwich Micro-Beam with Honeycomb Core And Piezoelectric/Porous Viscoelastic Graphene Facesheets

I. Safari[1], P. Pourmousa[1], E. Haghparast[1], S. Niknejad[1], A. Ghobanpour Arani [1,2*]

[1] *Faculty of Mechanical Engineering, University of Kashan, Kashan, Iran*[1]
[2] *Institute of Nanoscience & Nanotechnology, University of Kashan, Kashan, Iran*

Received 01 June 2020; Received in revised form 17 September 2020; Accepted 22 October 2020

ABSTRACT
In this paper, thermal dynamic stability analysis of sandwich microbeams made of a honeycomb core and piezoelectric and porous visco graphene sheets resting on visco Pasternak is studied. The microbeam is modeled based on the zigzag theory and in order to incorporate the size effect, strain gradient theory is utilized. The set of the governing equations are derived Hamilton's principle and are solved numerically using Galerkin method. The influences of various parameters on the thermal dynamic stability characteristics of the sandwich nanobeam are investigated including small scale, temperature changes, core to face sheets thickness ratio, intensity of electric fields and stiffness of elastic medium. The results of present work can be used to optimum design and control of micro-thermal/electro-mechanical devices.

Keywords: Thermal dynamics stability; Graphene; Honeycomb; Piezoelectric; Visco Pasternak foundation.

1 INTRODUCTION

RECENTLY, micro structures made of smart materials have been widely used in mechanical engineering [1-7] and military, aviation, marine and shipbuilding industries [8-10]. Therefore, there is a considerable number of works regarding mechanical analysis of structures in macro [11-17], micro [18-21] and nano [22-24] scales. Yoosefian et al. [25] studied nonlinear bending analysis of sandwich structures affected by thermal and mechanical loads. They showed that decrease in thickness ratio of the core reduces the radial stress. Using micro strain gradient theory and higher-order shear deformation beam theory, Al-shujairi and Mollamahmutoglu [26] investigated buckling and vibration analyses of sandwich microbeams under thermal load and resting on elastic foundation. They concluded that elastic foundation increases the critical buckling load and natural frequencies. Aria and Friswell [27]

*Corresponding author. Tel.: +98 31 55912450, Fax: +98 31 55912424.
E-mail address: aghorban@kashanu.ac.ir

studied thermal buckling and vibration analyses of sandwich microbeams. It was shown by them that temperature rise leads to reduction in natural frequencies and critical buckling load. Chen et al. [28] focused on the buckling analysis of sandwich structures with thermal sectional properties. Using first-order shear deformation theory (FSDT) and finite element method (FEM), dynamic response of the beams in a thermal environment was studied by Esen [29]. Ghorbanpour Arani et al. [30] studied free vibration analysis of sandwich microbeams resting on elastic foundation. They showed that vibration characteristics of sandwich composite microbeams with piezoelectric and piezomagnetic face sheets is controllable by the intensity of electric and magnetic fields [31-33]. Using strain gradient and surface stress elasticity theories, size-dependent vibration analysis of double-bonded isotropic piezoelectric Timoshenko microbeams under initial stress was investigated by Mohammadimehr et al. [34].

Due to the low density, honeycomb structurs have been used as the core in the sandwich structures in various fields to reduce the total weight of the structures like mechanics, civil and aerospace engineering [35]. Li et al. [36] and Liu et al. [37] studied thermal buckling analysis of sandwich beams with honeycomb core. Both negative Poisson's ratio and functionally graded configurations were taken into account which were the novelty of their work. The buckling and vibration analyses of sandwich beams in thermal environment were studied by Marynowski [38]. He studied the effect of the transport speed and the cover parameters on the dynamic behavior of the moving system in under-critical range of transport speed. Pradhan and Dash [39] studied stability analysis of sandwich beam subjected to thermal and mechanical axial loads. Waddar et al. [40] studied vibration and buckling analyses of sandwich beams under axial compressive load.

In this paper, thermal dynamic stability analysis of sandwich microbeams resting on visco Pasternak foundation is studied for the first time. In order to consider size effect strain gradient theory is employed and the microbeam is modeled based on the zigzag beam theory. The set of the governing equations are derived using Hamilton's principle are solved using Galerkin method. The effects of various parameters on the thermal dynamic stability characteristics of sandwich microbeam are investigated such as small scale parameter, temperature rise, core to face sheets thickness ratio, intensity of electric fields and stiffness and damping coefficients of the foundation.

Nevertheless, the review of literature confirms that no research has been carried out to study on the influence of porosity and viscoelastic behavior of graphene face sheets and temperature-dependent materials on the dynamic stability of five-layer microbeam based on zig-zag beam theory. Motivated by the aforementioned ideas, the presented study is conducted for the first time.

The result of this work can be useful to control and improve the performance of nano and micro devices which are employed in military equipment.

2 SANDWICH MICRO-BEAM MODELING

As depicted in Fig. 1, a sandwich microbeam of length L, width b and total thickness of h under the uniform electric field and resting on visco Pasternak foundation is considered. The microbeam is consisted of five layers including a honeycomb core of thicknesses h_m, two piezoelectric face sheets of thicknesses h_e and two visco graphene face sheets of thicknesses h_c.

According to the zigzag beam theory displacement field in the kth layer can be stated as [41]

$$u_1^k\left(x,z\right)=u\left(x\right)+z\theta\left(x\right)+\varphi^k\left(z\right)\psi\left(x\right), \tag{1}$$

$$u_3^k\left(x,z\right)=w\left(x\right), \tag{2}$$

where u_1 and u_3 are displacement along x and z directions, respectively; u and w are corresponding displacement at the mid-plane and θ and ψ stand for the bending rotation and amplitude of the zigzag displacement, respectively. Also φ^k is zigzag function which can be expressed as follows [42]:

$$\varphi^1\left(z\right)=\left(z+h\right)\left(\frac{G_s}{Q_{44}^k}-1\right) \tag{3}$$

$$\varphi^k\left(z\right)=\left(z+h\right)\left(\frac{G_s}{Q_{44}^k}-1\right)+\sum_{i=2}^{k}\left(\frac{G_1}{Q_{44}^{i-1}}-\frac{G_1}{Q_{44}^k}\right), \qquad k=2,3,\ldots \tag{4}$$

in which G_s and G_1 are shear moduli of the honeycomb core and Q^k_{44} is the shear modulus of the *k*th layer.
The strains associated with the displacement field in Eq. (1) are given by [43]:

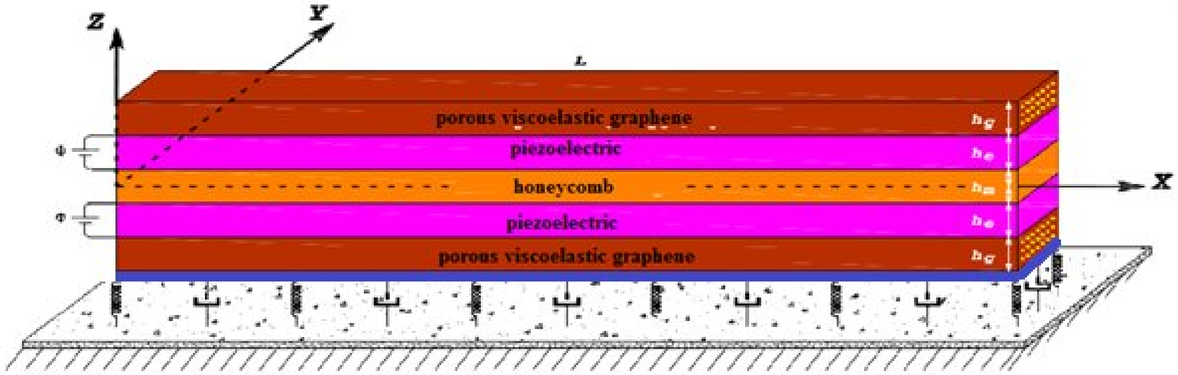

Fig. 1
Sandwich microbeam with honeycomb core and piezoelectric and porous viscoelastic graphene face sheets resting on visco Pasternak foundation.

$$\varepsilon_x = \frac{\partial U}{\partial x} = \frac{\partial u}{\partial x} + z\frac{\partial \theta}{\partial x} + \varphi^k(z)\frac{\partial \psi}{\partial x}, \tag{5}$$

$$\gamma_{xz} = \frac{\partial W}{\partial x} + \frac{\partial U}{\partial z} = \frac{\partial W}{\partial x} + \theta + \frac{d\varphi^k}{dz}\psi, \tag{6}$$

where ε_x and γ_{xz} are the normal and shear components of the strain tensor.

2.2. Piezoelectric layers

The constitutive equations for piezoelectric (Ti-6A1-4V) layers under electric field are given by [44]:

$$\begin{bmatrix}\sigma_{xx}\\ \sigma_{xz}\end{bmatrix}^e = \begin{bmatrix}Q_{11}(T) & 0\\ 0 & Q_{55}(T)\end{bmatrix}\begin{bmatrix}\varepsilon_x - \alpha\Delta T\\ \gamma_{xz}\end{bmatrix}^e + \begin{bmatrix}0 & e_{31}\\ 0 & 0\end{bmatrix}\begin{bmatrix}E_x\\ E_z\end{bmatrix}, \tag{11}$$

$$\begin{bmatrix}D_x\\ D_z\end{bmatrix} = \begin{bmatrix}0 & 0\\ 0 & e_{31}\end{bmatrix}\begin{bmatrix}\varepsilon_x\\ \gamma_{xz}\end{bmatrix}^e - \begin{bmatrix}h_{11} & 0\\ 0 & h_{33}\end{bmatrix}\begin{bmatrix}E_x\\ E_z\end{bmatrix}, \tag{12}$$

in which D_i, E_i, Q_{ij}, e_{ij}, h_{ij}, α and ΔT are the electric inductions, electric potential, elastic constants, piezoelectric constants and electric permeability coefficient, thermal expansion coefficient and temperature rise, respectively.

The piezoelectric stress constants can be obtained by using the piezoelectric strain and elastic constants as follows [44]:

$$\begin{bmatrix}0 & 0\\ e_{31} & 0\end{bmatrix} = \begin{bmatrix}0 & 0\\ d_{31} & 0\end{bmatrix}\begin{bmatrix}Q_{11}(T) & 0\\ 0 & Q_{55}(T)\end{bmatrix}, \tag{13}$$

where d_{31} is piezoelectric strain constant.

Distribution of electric potential along the thickness direction is supposed to be changed as a combination of a cosine as follows [45]:

$$\chi(x,z,t)=\begin{cases} -\cos\left[\dfrac{\pi}{h_e}\left(z-\dfrac{h_m}{2}\right)\right]\chi(x,t)+\dfrac{2}{h_e}\left(z-\dfrac{h_m}{2}\right)V_0\,e^{i\omega t} & \dfrac{h_m}{2}<z<\dfrac{h_m}{2}+h_e \\ -\cos\left[\dfrac{\pi}{h_e}\left(-z-\dfrac{h_m}{2}\right)\right]\chi(x,t)+\dfrac{2}{h_e}\left(-z-\dfrac{h_m}{2}\right)V_0\,e^{i\omega t} & -\dfrac{h_m}{2}-h_e<z<-\dfrac{h_m}{2} \end{cases}, \tag{14}$$

where ω and V_0 are the natural frequency of system and the initial external electric voltage, respectively. Therefore, the nonzero components of electric fields (E_x and E_z) can be written as [45]:

$$E_x=-\frac{\partial\chi}{\partial x}=\cos\left[\frac{\pi}{h_e}\left(z-\frac{h_m}{2}\right)\right]\frac{\partial\chi}{\partial x}, \tag{15a}$$

$$E_z=-\frac{\partial\chi}{\partial z}=-\frac{\pi}{h_e}\sin\left[\frac{\pi}{h_e}\left(z-\frac{h_m}{2}\right)\right]\chi. \tag{15b}$$

2.3. porous visco graphene face sheets

Material properties bottom (b) and top (t) face sheet can be written based on the symmetric pattern as [46-47]:

$$\begin{aligned}\begin{Bmatrix}E^t(z)\\G^t(z)\end{Bmatrix}&=\begin{Bmatrix}E_1\\G_1\end{Bmatrix}\left\{1-\zeta\cos\left[\tfrac{\pi}{h_g}\left(z-\tfrac{h_m}{2}-h_e-\tfrac{h_g}{2}\right)\right]\right\}\\ \rho^t(z)&=\rho_1\left\{1-\xi\cos\left[\tfrac{\pi}{h_g}\left(z-\tfrac{h_m}{2}-h_e-\tfrac{h_g}{2}\right)\right]\right\}\end{aligned} \tag{16}$$

$$\begin{aligned}\begin{Bmatrix}E^b(z)\\G^b(z)\end{Bmatrix}&=\begin{Bmatrix}E_1\\G_1\end{Bmatrix}\left\{1-\xi\cos\left[\tfrac{\pi}{h_g}\left(z+\tfrac{h_m}{2}+h_e+\tfrac{h_g}{2}\right)\right]\right\}\\ \rho^b(z)&=\rho_1\left\{1-\xi\cos\left[\tfrac{\pi}{h_g}\left(z+\tfrac{h_m}{2}+h_e+\tfrac{h_g}{2}\right)\right]\right\}\end{aligned} \tag{17}$$

where ζ denoted porosity index and ξ described mass density which can be written as [48]

$$\xi=1-\sqrt{1-\zeta} \tag{18}$$

Stress in FG visco Porous graphene can be defined as [49]

$$\begin{bmatrix}\sigma_{xx}\\\sigma_{xz}\end{bmatrix}=\begin{bmatrix}\tilde{Q}_{11}(T)&0\\0&\tilde{Q}_{55}(T)\end{bmatrix}\begin{bmatrix}\varepsilon_x-\alpha\Delta T\\\gamma_{xz}\end{bmatrix}, \tag{19}$$

where

$$\tilde{Q}_{11}(T)=Q_{ij}(T)\left(1+g\frac{\partial}{\partial t}\right) \tag{20}$$

in which g is visco coefficient and Q_{ij} is defined as follows [49]:

$$Q_{11}=\frac{E}{1-\nu},Q_{55}=G_{12}, \tag{21}$$

in which E and G_{12} represent elastic and shear moduli, respectively.

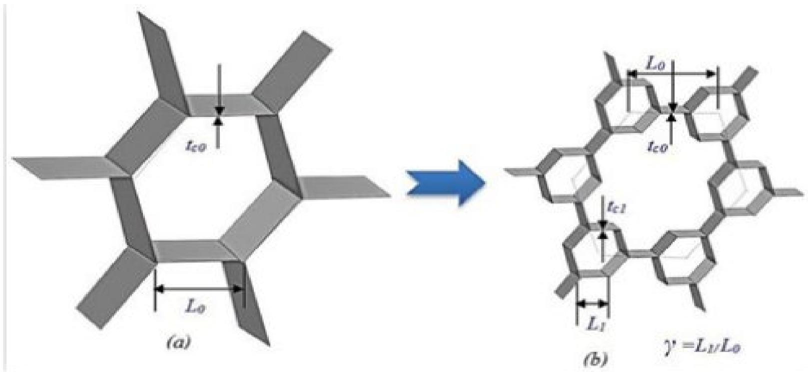

Fig. 2
Honeycomb structure cell (a) regular (b) 1st order hierarchy [50].

2.4. Honeycomb core

In Figure 2 a typical honeycomb cell with its parameters is depicted. It is supposed in this paper that the hexagonal honeycomb core is made of Aluminum.

The relative material properties of the honeycomb structure can be calculated as [51-52]

$$\rho^C = \frac{2\rho^* t_{co}}{\sqrt{3}L_0}\left(1+2\gamma\right), \tag{22}$$

$$E^C = \frac{4E^*}{\sqrt{3}}\left(\frac{t_{co}}{L_0}\right)^3 \frac{1}{1-4.7\gamma+4.8\gamma^2+3.78\gamma^3} \tag{23}$$

$$\nu^C = \nu^*\left(1-\frac{1}{0.75-3.525\gamma+3.6\gamma^2+2.9\gamma^3}\right) \tag{24}$$

where ρ^*, E^* and ν^* are the density, Young's modulus and Poisson's ratio of the material and γ is defined as follows [50]:

$$\gamma = \frac{L_1}{L_0} \tag{25}$$

3 HAMILTON'S PRINCIPLE

The set of the governing equations for the dynamic analysis of sandwich microbeam restingg on visco Pasternak foundation can be derived using Hamilton's principle as follows [53]:

$$\delta\int_{t_1}^{t_2}\left[U-\left(K+\Sigma\right)\right]dt = 0 \tag{26}$$

in which U, K and Σ are strain energy, kinetic energy and work done by external loads, respectively.
The energy U that occupying region Λ is given as [54]:

$$U = \frac{1}{2}\int_{\Lambda}\left(\sigma_{ij}\varepsilon_{jk} - D_i E_i + p_i\gamma_i + \tau_{ijk}^{(1)}\eta_{ijk}^{(1)} + m_{ij}\chi_{ij}\right)d\Lambda, \tag{27}$$

in which γ_i, $\eta_{ijk}^{(1)}$ and χ_{ij} represent the dilatation gradient vector, deviatoric stretch gradient and symmetric rotation gradient tensors, respectively and p_i, $\tau_{ijk}^{(1)}$ and m_{ij} are the higher-order stresses. These terms are defined as follows [54]:

$$\varepsilon_{ij} = \frac{1}{2}\left(\frac{\partial u_j}{\partial x_i} + \frac{\partial u_i}{\partial x_j}\right), \tag{28}$$

$$\gamma_i = \frac{\partial \varepsilon_{mm}}{\partial x_i}, \tag{29}$$

$$\eta_{ijk}^{(1)} = \frac{1}{3}\left(\frac{\partial \varepsilon_{jk}}{\partial x_i} + \frac{\partial \varepsilon_{ki}}{\partial x_j} + \frac{\partial \varepsilon_{ij}}{\partial x_k}\right) - \frac{1}{15}\left[\delta_{ij}\left(\frac{\partial \varepsilon_{mm}}{\partial x_k} + 2\frac{\partial \varepsilon_{mk}}{\partial x_m}\right) + \delta_{jk}\left(\frac{\partial \varepsilon_{mm}}{\partial x_i} + 2\frac{\partial \varepsilon_{mi}}{\partial x_m}\right) + \delta_{ki}\left(\frac{\partial \varepsilon_{mm}}{\partial x_j} + 2\frac{\partial \varepsilon_{mj}}{\partial x_m}\right)\right], \tag{30}$$

$$\chi_{ij} = \frac{1}{2}\left(e_{ipq}\frac{\partial \varepsilon_{qj}}{\partial x_p} + e_{jpq}\frac{\partial \varepsilon_{qi}}{\partial x_p}\right), \tag{31}$$

$$p_i = 2{l_0}^2 G\gamma_{i,} \tag{32}$$

$$\tau_{ijk}^{(1)} = 2{l_1}^2 G\eta_{ijk}^{(1)}, \tag{33}$$

$$m_{ij} = 2{l_2}^2 G\chi_{ij}, \tag{34}$$

where u_i, δ_{ij} and e_{ipq} are the displacement vector, well-known kronecker delta and alternate tensor, respectively and l_0, l_1 and l_2 indicate to the three material length scale parameters.

Using Eqs. (5) and (6), the terms appeared in Eqs. (27-34) can be written in a expanded form presented in Appendix A.

The strain energy of the each layer of the nanobeam can be stated as [53]

$$U_{honeycomb\ core} = \frac{1}{2}\int_0^L \int_{-\frac{h_m}{2}}^{\frac{h_m}{2}} \left(\sigma_{ij}^m \varepsilon_{jk}^m + p_i\gamma_i + \tau_{ijk}^{(1)}\eta_{ijk}^{(1)} + m_{ij}\chi_{ij}\right) dz\, dx, \tag{35}$$

$$\begin{aligned} U_{piezoelectric} = &\frac{1}{2}\int_0^L \int_{\frac{h_m}{2}}^{\frac{h_m}{2}+h_e} \left(\sigma_{ij}^e \varepsilon_{jk}^e - D_i E_i + p_i\gamma_i + \tau_{ijk}^{(1)}\eta_{ijk}^{(1)} + m_{ij}\chi_{ij}\right) dz\, dx \\ &+ \frac{1}{2}\int_0^L \int_{-\frac{h_m}{2}-h_e}^{-\frac{h_m}{2}} \left(\sigma_{ij}^e \varepsilon_{jk}^e - D_i E_i + p_i\gamma_i + \tau_{ijk}^{(1)}\eta_{ijk}^{(1)} + m_{ij}\chi_{ij}\right) dz\, dx, \end{aligned} \tag{36}$$

$$\begin{aligned} U_{graphene} = &\frac{1}{2}\int_0^L \int_{\frac{h_m}{2}+h_e}^{\frac{h_m}{2}+h_e+h_c} \left(\sigma_{ij}^c \varepsilon_{jk}^c + p_i\gamma_i + \tau_{ijk}^{(1)}\eta_{ijk}^{(1)} + m_{ij}\chi_{ij}\right) dz\, dx \\ &+ \frac{1}{2}\int_0^L \int_{-\frac{h_m}{2}-h_e-h_c}^{-\frac{h_m}{2}-h_e} \left(\sigma_{ij}^c \varepsilon_{jk}^c + p_i\gamma_i + \tau_{ijk}^{(1)}\eta_{ijk}^{(1)} + m_{ij}\chi_{ij}\right) dz\, dx, \end{aligned} \tag{37}$$

and the kinetic energy can be written as following form [54-55]:

$$K_{piezomagnet} = \frac{1}{2}\int_0^L \int_{-\frac{h_m}{2}}^{\frac{h_m}{2}} \rho_m \left[\left(\frac{\partial U}{\partial t}\right)^2 + \left(\frac{\partial W}{\partial t}\right)^2\right] dz\, dx, \tag{38}$$

$$K_{piezoelectric}=\frac{1}{2}\int_0^L\int_{\frac{h_m}{2}}^{\frac{h_m}{2}+h_e}\rho_e\left[\left(\frac{\partial U}{\partial t}\right)^2+\left(\frac{\partial W}{\partial t}\right)^2\right]dz\,dx+\frac{1}{2}\int_0^L\int_{-\frac{h_m}{2}-h_e}^{-\frac{h_m}{2}}\rho_e\left[\left(\frac{\partial U}{\partial t}\right)^2+\left(\frac{\partial W}{\partial t}\right)^2\right]dz\,dx, \tag{39}$$

$$K_{graphene}=\frac{1}{2}\int_0^L\int_{\frac{h_m}{2}+h_e}^{\frac{h_m}{2}+h_e+h_c}\rho_c\left[\left(\frac{\partial U}{\partial t}\right)^2+\left(\frac{\partial W}{\partial t}\right)^2\right]dz\,dx+\frac{1}{2}\int_0^L\int_{-\frac{h_m}{2}-h_e-h_c}^{-\frac{h_m}{2}-h_e}\rho_c\left[\left(\frac{\partial U}{\partial t}\right)^2+\left(\frac{\partial W}{\partial t}\right)^2\right]dz\,dx, \tag{40}$$

in which ρ_c,ρ_e,ρ_g stand for density of the core, piezoelectric layers and graphene layers, respectively.

Substituting Eqs. (35)-(40) into Eq. (26) and using Eqs (A-1)-(A-21) leads to the following ste of the governing equations:

$c = honeycomb\ core, p = piezoelectric$, g $= graphene, t\ or\ b = top\ and\ bottom\ sheet$

$$\begin{aligned}
su ={}& -C_{11}I_{0c}\frac{\partial^2 u}{\partial x^2}-C_{11}I_{1c}\frac{\partial^2\theta}{\partial x^2}+I_{0c}\rho_c\frac{\partial^2 u}{\partial t^2}+I_{1c}\rho_c\frac{\partial^2\theta}{\partial t^2}+\rho_c I_{9c}\frac{\partial^2\psi}{\partial t^2}(x,t)-\frac{e_{31}I_{29pi}\pi}{h_e}\left(\frac{\partial\beta}{\partial x}\right)\\
&-C_{11}I_{0pi}\frac{\partial^2 u}{\partial x^2}-C_{11}I_{1pi}\frac{\partial^2\theta}{\partial x^2}+I_{0pi}\rho_e\frac{\partial^2 u}{\partial t^2}+I_{1pi}\rho_e\frac{\partial^2\theta}{\partial t^2}-C_{11}I_{9pi}\frac{\partial^2\psi}{\partial x^2}+\rho_e I_{9pi}\frac{\partial^2\psi}{\partial t^2}\\
&-I_{19gi}\left(\frac{\partial^2 u}{\partial x^2}\right)-I_{13gi}\frac{\partial^2\theta}{\partial x^2}+I_{3gi}\frac{\partial^2 u}{\partial t^2}+I_{4gi}\frac{\partial^2\theta}{\partial t^2}-I_{15gi}\frac{\partial^2\psi}{\partial x^2}+I_{5gi}\frac{\partial^2\psi}{\partial t^2}-gI_{19pi}\frac{\partial^3 u}{\partial x^2\partial t}-gI_{13pi}\frac{\partial^3\theta}{\partial x^2\partial t}\\
&-I_{15gi}\,g\frac{\partial^3\psi}{\partial x^2\partial t}l_0^2GI_{0c}\frac{\partial^4 u}{\partial x^4}+2l_0^2GI_{1c}\frac{\partial^4\theta}{\partial x^4}+\frac{4}{5}l_1^2GI_{0c}\frac{\partial^4 u}{\partial x^4}+\frac{4}{5}l_1^2I_{1c}G\frac{\partial^4\theta}{\partial x^4}l_0^2GI_{0p}\frac{\partial^4 u}{\partial x^4}\\
&+2l_0^2GI_{1p}\frac{\partial^4\theta}{\partial x^4}+\frac{4}{5}l_1^2GI_{0p}\frac{\partial^4 u}{\partial x^4}+\frac{4}{5}l_1^2I_{1p}G\frac{\partial^4\theta}{\partial x^4}+l_0^2GI_{0g}\frac{\partial^4 u}{\partial x^4}+2l_0^2GI_{1g}\frac{\partial^4\theta}{\partial x^4}+\frac{4}{5}l_1^2GI_{0g}\frac{\partial^4 u}{\partial x^4}\\
&+\frac{4}{5}l_1^2I_{1g}G\frac{\partial^4\theta}{\partial x^4}+\frac{4}{5}l_1^2GI_{9c}\frac{\partial^4\psi}{\partial x^4}+2l_0^2GI_{9c}\frac{\partial^4\psi}{\partial x^4}-\frac{4}{5}l_1^2GI_{22c}\frac{\partial^2\psi}{\partial x^2}+\frac{4}{5}l_1^2GI_{9p}\frac{\partial^4\psi}{\partial x^4}\\
&+2l_0^2GI_{9p}\frac{\partial^4\psi}{\partial x^4}-\frac{4}{5}l_1^2GI_{22p}\frac{\partial^2\psi}{\partial x^2}-\frac{4}{5}l_1^2GI_{9g}\frac{\partial^4\psi}{\partial x^4}+2l_0^2GI_{9g}\frac{\partial^4\psi}{\partial x^4}-\frac{4}{5}l_1^2GI_{22g}\frac{\partial^2\psi}{\partial x^2}=0,
\end{aligned} \tag{41}$$

$$
\begin{aligned}
& s\psi = k_s I_{11c}\frac{\partial w}{\partial x} + k_s I_{20c}\psi - C_{11}I_{23c}\frac{\partial^2\psi}{\partial x^2} + k_s C_{55c}I_{11c}\theta - k_s C_{55}I_{20c}\psi + k_s C_{55}I_{11c}\frac{\partial w}{\partial x} \\
& -\rho_c I_{9c}\frac{\partial^2 u}{\partial t^2} + \rho_c I_{26c}\frac{\partial^2\theta}{\partial t^2} + \rho_c I_{23c}\frac{\partial^2\psi}{\partial t^2} - C_{11}I_{4pi}\frac{\partial^2\theta}{\partial x^2} - C_{11}I_{23pi}\frac{\partial^2\psi}{\partial x^2} - C_{11}I_{9pi}\frac{\partial^2 u}{\partial x^2} \\
& +k_s C_{55}I_{11pi}\theta + k_s C_{55}I_{20pi}\psi + k_s C_{55}I_{11pi}\frac{\partial w}{\partial x} - \frac{\pi e_{31}I_{33pi}}{h_e}(\frac{\partial\beta}{\partial x}) + \rho_e I_{9pi}\frac{\partial^2 u}{\partial t^2} + \rho_e I_{26pi}\frac{\partial^2\theta}{\partial t^2} \\
& +\rho_e I_{23pi}\frac{\partial^2\psi}{\partial t^2} + k_s I_{18gi}\frac{\partial w}{\partial x} + k_s I_{18gi}\theta + k_s I_{21gi}\psi - I_{15gi}\frac{\partial^2 u}{\partial x^2} - I_{13gi}\frac{\partial^2\theta}{\partial x^2} - I_{17gi}\frac{\partial^2\psi}{\partial x^2} + I_{5gi}\frac{\partial^2 u}{\partial t^2} \\
& +I_{7gi}\frac{\partial^2\theta}{\partial t^2} + I_{8gi}\frac{\partial^2\psi}{\partial t^2} - I_{13gi}\frac{\partial^3\theta}{\partial x^2\partial t} - I_{17gi}\frac{\partial^3\psi}{\partial x^2\partial t} + k_s I_{18gi}\frac{\partial^2 w}{\partial x\partial t} + k_s I_{18gi}\frac{\partial\theta}{\partial t} + k_s I_{21gi}\frac{\partial\psi}{\partial t} \\
& -I_{15gi}\frac{\partial^3 u}{\partial x^2\partial t} + k_s I_{18gi}\, g\frac{\partial^2 w}{\partial x\partial t} + k_s I_{18gi}\, g\frac{\partial\theta}{\partial t} + k_s I_{21gi}\, g\frac{\partial\psi}{\partial t} - I_{15gi}\, g\frac{\partial^3 u}{\partial x^2\partial t} - I_{13gi}\, g\frac{\partial^3\theta}{\partial x^2\partial t} \\
& -I_{17gi}\, g\frac{\partial^3\psi}{\partial x^2\partial t} - \frac{16}{5}l_1^2 GI_{11g}\frac{\partial^3 w}{\partial x^3} - \frac{1}{8}l_2^2 GI_{20g}\frac{\partial^2\psi}{\partial x^2} - \frac{8}{5}l_1^2 GI_{25c}\frac{\partial^2\psi}{\partial x^2} + \frac{1}{8}l_2^2 GI_{11c}\frac{\partial^3 w}{\partial x^3} \\
& -2l_0^2 GI_{11c}\frac{\partial^2\theta}{\partial x^2} - \frac{24}{5}l_1^2 I_{11c}G\frac{\partial^2\theta}{\partial x^2} - \frac{4}{5}l_1^2 GI_{22c}\frac{\partial^2 u}{\partial x^2} + \frac{32}{15}l_1^2 GI_{22c}\psi + \frac{1}{8}l_2^2 GI_{22c}\psi \\
& +\frac{4}{5}l_1^2 GI_{26c}\frac{\partial^4}{\partial x^4}\theta + 2l_0^2 GI_{9c}\frac{\partial^4 u}{\partial x^4} - \frac{4}{5}l_1^2 GI_{24c}\frac{\partial^2\theta}{\partial x^2} + \frac{4}{5}l_1^2 GI_{9c}\frac{\partial^4 u}{\partial x^4} + \frac{4}{5}l_1^2 GI_{23c}\frac{\partial^4\psi}{\partial x^4} \\
& +2l_0^2 GI_{23c}\frac{\partial^4\psi}{\partial x^4} + 2l_0^2 GI_{26c}\frac{\partial^4\theta}{\partial x^4} - \frac{24}{5}l_1^2 GI_{20c}\frac{\partial^2\psi}{\partial x^2} - 2l_0^2 GI_{20c}\frac{\partial^2\psi}{\partial x^2} - \frac{1}{8}l_2^2 I_{11c}G\frac{\partial^2\theta}{\partial x^2} \\
& -\frac{16}{5}l_1^2 GI_{11c}\frac{\partial^3 w}{\partial x^3} - \frac{1}{8}l_2^2 GI_{20c}\frac{\partial^2\psi}{\partial x^2} - 2l_0^2 GI_{20g}\frac{\partial^2\psi}{\partial x^2} - \frac{8}{5}l_1^2 GI_{25p}\frac{\partial^2\psi}{\partial x^2} + \frac{1}{8}l_2^2 GI_{11p}\frac{\partial^3 w}{\partial x^3} \\
& -2l_0^2 GI_{11p}\frac{\partial^2\theta}{\partial x^2} - \frac{24}{5}l_1^2 I_{11p}G\frac{\partial^2\theta}{\partial x^2} - \frac{4}{5}l_1^2 GI_{22p}\frac{\partial^2 u}{\partial x^2} + \frac{32}{15}l_1^2 GI_{22p}\psi + \frac{1}{8}l_2^2 GI_{22p}\psi \\
& +\frac{4}{5}l_1^2 GI_{26p}\frac{\partial^4\theta}{\partial x^4} + 2l_0^2 GI_{9p}\frac{\partial^4 u}{\partial x^4} - \frac{4}{5}l_1^2 GI_{24p}\frac{\partial^2\theta}{\partial x^2} + \frac{4}{5}l_1^2 GI_{9p}\frac{\partial^4 u}{\partial x^4} + \frac{4}{5}l_1^2 GI_{23p}\frac{\partial^4\psi}{\partial x^4} \\
& +2l_0^2 GI_{23p}\frac{\partial^4\psi}{\partial x^4} + 2l_0^2 GI_{26p}\frac{\partial^4\theta}{\partial x^4} - \frac{24}{5}l_1^2 GI_{20p}\frac{\partial^2\psi}{\partial x^2} - 2l_0^2 GI_{20p}\frac{\partial^2\psi}{\partial x^2} - \frac{1}{8}l_2^2 I_{11p}G\frac{\partial^2\theta}{\partial x^2} \\
& -\frac{16}{5}l_1^2 GI_{11p}\frac{\partial^3 w}{\partial x^3} - \frac{1}{8}l_2^2 GI_{20p}\frac{\partial^2\psi}{\partial x^2} - \frac{24}{5}l_1^2 GI_{20g}\frac{\partial^2\psi}{\partial x^2} - \frac{8}{5}l_1^2 GI_{25g}\frac{\partial^2\psi}{\partial x^2} + \frac{1}{8}l_2^2 GI_{11g}\frac{\partial^3 w}{\partial x^3} \\
& -2l_0^2 GI_{11g}\frac{\partial^2\theta}{\partial x^2} - \frac{24}{5}l_1^2 I_{11g}G\frac{\partial^2\theta}{\partial x^2} - \frac{4}{5}l_1^2 GI_{22g}\frac{\partial^2 u}{\partial x^2} + \frac{32}{15}l_1^2 GI_{22g}\psi + \frac{1}{8}l_2^2 GI_{22g}\psi \\
& +\frac{4}{5}l_1^2 GI_{26g}\frac{\partial^4\theta}{\partial x^4} + 2l_0^2 GI_{9g}\frac{\partial^4 u}{\partial x^4} - \frac{4}{5}l_1^2 GI_{24g}\frac{\partial^2\theta}{\partial x^2} + \frac{4}{5}l_1^2 GI_{9g}\frac{\partial^4 u}{\partial x^4} + \frac{4}{5}l_1^2 GI_{23g}\frac{\partial^4\psi}{\partial x^4} \\
& +2l_0^2 GI_{23g}\frac{\partial^4\psi}{\partial x^4} + 2l_0^2 GI_{26g}\frac{\partial^4\theta}{\partial x^4} - \frac{1}{8}l_2^2 I_{11g}G\frac{\partial^2\theta}{\partial x^2} = 0,
\end{aligned} \tag{42}
$$

$$
\begin{aligned}
& s\theta = k_s I_{0c}\frac{\partial w}{\partial x} + k_s I_{0c}\theta - C_{11}I_{1c}\frac{\partial^2 u}{\partial x^2} - C_{11}I_{2c}\frac{\partial^2\theta}{\partial x^2} + 2l_0^2 GI_{26g}\frac{\partial^4\psi}{\partial x^4} + I_{1c}\rho_c\frac{\partial^2 u}{\partial t^2} \\
& +\rho_c I_{2c}\frac{\partial^2\theta}{\partial t^2} + k_s C_{55}I_{11c}\psi + \rho_c I_{26c}\frac{\partial^2\psi}{\partial t^2} - \frac{24}{5}l_1^2 I_{11g}G\frac{\partial^2\psi}{\partial x^2} - \left(\frac{e_{31}I_{30pi}\pi}{h_e}\right)\frac{\partial\beta}{\partial x} \\
& +k_s I_{0pi}C_{55}\frac{\partial w}{\partial x} + k_s I_{0pi}C_{55}\theta - C_{11}I_{1pi}\frac{\partial^2 u}{\partial x^2} + \frac{1}{2}C_{11}I_{2pi}\frac{\partial^2\theta}{\partial x^2} + I_{1pi}\rho_e\frac{\partial^2 u}{\partial t^2} + \rho_e I_{2pi}\frac{\partial^2\theta}{\partial t^2} \\
& -C_{11}I_{4pi}\frac{\partial^2\psi}{\partial x^2} + k_s C_{55}I_{11pi}\psi + \rho_c I_{26pi}\frac{\partial^2\psi}{\partial t^2} + k_s I_{12gi}\frac{\partial w}{\partial x} + k_s I_{12gi}\theta - I_{14gi}\frac{\partial^2 u}{\partial x^2} - I_{16gi}\frac{\partial^2\theta}{\partial x^2} \\
& +I_{4gi}\frac{\partial^2 u}{\partial t^2} + I_{6gi}\frac{\partial^2\theta}{\partial t^2} + k_s I_{18gi}\psi - I_{16gi}\frac{\partial^2\theta}{\partial x^2} - I_{13gi}\frac{\partial^2\psi}{\partial x^2} + I_{7gi}\frac{\partial^2\psi}{\partial t^2} + k_s I_{12gi}g\frac{\partial^2 w}{\partial x\,\partial t} \\
& +k_s I_{12gi}g\frac{\partial\theta}{\partial t} - I_{14gi}g\frac{\partial^3 u}{\partial x^2\partial t} - I_{16gi}g\frac{\partial^3\theta}{\partial x^2\partial t} + k_s I_{18gi}g\frac{\partial\psi}{\partial t} - I_{13gi}g\frac{\partial^3\psi}{\partial x^2\partial t} + \frac{1}{8}l_2^2 GI_{0c}\frac{\partial^3 w}{\partial x^3} \\
& -\frac{1}{8}l_2^2 GI_{0c}\frac{\partial^2\theta}{\partial x^2} + 2l_0^2 GI_{1c}\frac{\partial^4 u}{\partial x^4} + 2l_0^2 GI_{2c}\frac{\partial^4\theta}{\partial x^4} - 2l_0^2 GI_{0c}\frac{\partial^2\theta}{\partial x^2} + \frac{4}{5}l_1^2 I_{1c}G\frac{\partial^4 u}{\partial x^4} \\
& +\frac{4}{5}l_1^2 GI_{2c}\frac{\partial^4\theta}{\partial x^4} - \frac{16}{5}l_1^2 GI_{0c}\frac{\partial^3 w}{\partial x^3} - \frac{24}{5}l_1^2 GI_{0c}\frac{\partial^2\theta}{\partial x^2} + \frac{1}{8}l_2^2 GI_{0p}\frac{\partial^3 w}{\partial x^3} - \frac{1}{8}l_2^2 GI_{0p}\frac{\partial^2\theta}{\partial x^2} \\
& +2l_0^2 GI_{1p}\frac{\partial^4 u}{\partial x^4} + 2l_0^2 GI_{2p}\frac{\partial^4\theta}{\partial x^4} - 2l_0^2 GI_{0p}\frac{\partial^2\theta}{\partial x^2} + \frac{4}{5}l_1^2 I_{1p}G\frac{\partial^4 u}{\partial x^4} + \frac{4}{5}l_1^2 GI_{2p}\frac{\partial^4\theta}{\partial x^4} \\
& -\frac{16}{5}l_1^2 GI_{0p}\frac{\partial^3 w}{\partial x^3} - \frac{24}{5}l_1^2 GI_{0p}\frac{\partial^2\theta}{\partial x^2} - \frac{24}{5}l_1^2 GI_{0g}\frac{\partial^2\theta}{\partial x^2} + \frac{1}{8}l_2^2 GI_{0g}\frac{\partial^3 w}{\partial x^3} - \frac{1}{8}l_2^2 GI_{0g}\frac{\partial^2\theta}{\partial x^2} \\
& +2l_0^2 GI_{1g}\frac{\partial^4 u}{\partial x^4} - \frac{16}{5}l_1^2 GI_{0g}\frac{\partial^3 w}{\partial x^3} + 2l_0^2 GI_{2g}\frac{\partial^4\theta}{\partial x^4} - 2l_0^2 GI_{0g}\frac{\partial^2\theta}{\partial x^2} + \frac{4}{5}l_1^2 I_{1g}G\frac{\partial^4 u}{\partial x^4} \\
& +\frac{4}{5}l_1^2 GI_{2g}\frac{\partial^4\theta}{\partial x^4} + \frac{4}{5}l_1^2 GI_{26c}\frac{\partial^4\psi}{\partial x^4} - 2l_0^2 GI_{11c}\frac{\partial^2\psi}{\partial x^2} - \frac{4}{5}l_1^2 GI_{24c}\frac{\partial^2\psi}{\partial x^2} - \frac{1}{8}l_2^2 I_{11c}G\frac{\partial^2\psi}{\partial x^2} \\
& -\frac{24}{5}l_1^2 I_{11c}G\frac{\partial^2\psi}{\partial x^2} + 2l_0^2 GI_{26c}\frac{\partial^4\psi}{\partial x^4} + \frac{4}{5}l_1^2 GI_{26p}\frac{\partial^4\psi}{\partial x^4} - 2l_0^2 GI_{11p}\frac{\partial^2\psi}{\partial x^2} \\
& -\frac{4}{5}l_1^2 GI_{24p}\frac{\partial^2\psi}{\partial x^2} - \frac{1}{8}l_2^2 I_{11p}G\frac{\partial^2\psi}{\partial x^2} - \frac{24}{5}l_1^2 I_{11p}G\frac{\partial^2\psi}{\partial x^2} + 2l_0^2 GI_{26p}\frac{\partial^4\psi}{\partial x^4} \\
& \frac{4}{5}l_1^2 GI_{26g}\frac{\partial^4\psi}{\partial x^4} - 2l_0^2 GI_{11g}\frac{\partial^2\psi}{\partial x^2} - \frac{4}{5}l_1^2 GI_{24g}\frac{\partial^2\psi}{\partial x^2} - \frac{1}{8}l_2^2 I_{11g}G\frac{\partial^2\psi}{\partial x^2} = 0
\end{aligned}
\tag{43}
$$

$$
\begin{aligned}
sw =& -I_{0c} k_s \frac{\partial^2 w}{\partial x^2} - k_s I_{0c} \frac{\partial \theta}{\partial x} - k_w w + k_G \frac{\partial^2 w}{\partial x^2} - C_d \frac{\partial w}{\partial t} + N_T \frac{\partial^2 w}{\partial x^2} + N_x \frac{\partial^2 w}{\partial x^2} \\
&+ I_{0c} \rho_c \frac{\partial^2 w}{\partial t^2} - k_s C_{55} I_{11} \frac{\partial \psi}{\partial x} - k_s I_{0pi} C_{55} \frac{\partial^2 w}{\partial x^2} - k_s I_{0pi} C_{55} \frac{\partial \theta}{\partial x} + I_{0pi} \rho_e \frac{\partial^2 w}{\partial t^2} \\
&- k_s C_{55} I_{11pi} \frac{\partial \psi}{\partial x} - I_{12gi} k_s \frac{\partial^2 w}{\partial x^2} - k_s I_{12gi} \frac{\partial \theta}{\partial x} + I_{3gi} \frac{\partial^2 w}{\partial t^2} w - k_s I_{18gi} \frac{\partial \psi}{\partial x} \\
&- k_s I_{12gi}\, g \frac{\partial^3 w}{\partial x^2 \partial t} - k_s I_{12pi}\, g \frac{\partial^2 \theta}{\partial x\, \partial t} - k_s I_{18gi}\, g \frac{\partial^2 \psi}{\partial x\, \partial t} + \frac{1}{8} l_2^2 G I_{0c} \frac{\partial^4 w}{\partial x^4} - \frac{1}{8} l_2^2 G I_{0c} \frac{\partial^3 \theta}{\partial x^3} \\
&+ \frac{32}{15} l_1^2 G I_{0c} \frac{\partial^4 w}{\partial x^4} + \frac{16}{5} l_1^2 G I_{0c} \frac{\partial^3 \theta}{\partial x^3} + \frac{1}{8} l_2^2 G I_{0p} \frac{\partial^4 w}{\partial x^4} - \frac{1}{8} l_2^2 G I_{0p} \frac{\partial^3 \theta}{\partial x^3} + \frac{32}{15} l_1^2 G I_{0p} \frac{\partial^4 w}{\partial x^4} \\
&+ \frac{16}{5} l_1^2 G I_{0p} \frac{\partial^3 \theta}{\partial x^3} + \frac{1}{8} l_2^2 G I_{0g} \frac{\partial^4 w}{\partial x^4} - \frac{1}{8} l_2^2 G I_{0g} \frac{\partial^3 \theta}{\partial x^3} + \frac{32}{15} l_1^2 G I_{0g} \frac{\partial^4 w}{\partial x^4} + \frac{16}{5} l_1^2 G I_{0g} \frac{\partial^3 \theta}{\partial x^3} \\
&- \frac{1}{8} l_2^2 G I_{11c} \frac{\partial^3 \psi}{\partial x^3} - \frac{16}{5} l_1^2 G I_{11c} \frac{\partial^3 \psi}{\partial x^3} - \frac{1}{8} l_2^2 G I_{11p} \frac{\partial^3 \psi}{\partial x^3} - \frac{16}{5} l_1^2 G I_{11p} \frac{\partial^3 \psi}{\partial x^3} - \frac{1}{8} l_2^2 G I_{11g} \frac{\partial^3 \psi}{\partial x^3} \\
&- \frac{16}{5} l_1^2 G I_{11g} \frac{\partial^3 \psi}{\partial x^3} = 0;
\end{aligned}
\tag{44}
$$

$$
\begin{aligned}
s\beta =& I_{27} h_{11} \frac{\partial^2 \beta}{\partial x^2} + I_{34} e_{15} \frac{\partial^2 w}{\partial x^2} + e_{15} I_{34} \frac{\partial \theta}{\partial x} - \left(\frac{h_{33} I_{28} \pi^2}{h_e^2}\right) \chi + \left(\frac{e_{31} I_{29} \pi}{h_e}\right) \frac{\partial u}{\partial x} \\
&+ \left(\frac{e_{31} I_{30} \pi}{h_e}\right) \frac{\partial \theta}{\partial x} + \frac{\pi e_{31} I_{33}}{h_e} \frac{\partial \beta}{\partial x} = 0,
\end{aligned}
\tag{45}
$$

where I_i is defined in Appendix B in which subscripts c, p, g stand for honeycomb core, piezoelectric layer and graphene layer respectively. Also, k_s, N_x^e and N^T are shear correction factor, normal forces induced external electric voltage and thermal load, respectively, which are defined as follows [30,56]:

$$N_x^e = -2 e_{31} V_0 \tag{46}$$

$$N_c^T = \int E_c \alpha \Delta T dz \tag{47}$$

$$N_e^T = \int E_e \alpha \Delta T dz \tag{48}$$

$$N_g^T = \int E_g \alpha \Delta T dz \tag{49}$$

$$N^T = 2N_g^T + 2N_e^T + N_m^T \tag{50}$$

Also, boundary conditions can be stated as follows:

$$
\begin{aligned}
&u=0 \quad or \qquad EI\frac{\partial u}{\partial x}=0\\
&w=0 \quad or \quad k_s AG\left(\frac{\partial w}{\partial x}-\theta\right)=0\\
&\theta=0 \quad or \qquad EI\frac{\partial \theta}{\partial x}=0
\end{aligned} \tag{51}
$$

4 SOLUTION METHOD

For simply supported sandwich microbeam, the following solution can be considered [57]:

$$U(\mathrm{x},\mathrm{t})=\sum_{m=1}^{\infty}U_m(t)\cos(\lambda x), \tag{52}$$

$$\mathrm{W}(\mathrm{x},\mathrm{t})=\sum_{m=1}^{\infty}w_m(t)\sin(\lambda x), \tag{53}$$

$$\psi(\mathrm{x},\mathrm{t})=\sum_{m=1}^{\infty}\psi_m(t)\cos(\lambda x), \tag{54}$$

$$\theta(\mathrm{x},\mathrm{t})=\sum_{m=1}^{\infty}\theta_m(t)\cos(\lambda x), \tag{55}$$

$$N_T(\mathrm{x},\mathrm{t})=\sum_{m=1}^{\infty}N_T(t)\sin(\lambda x), \tag{56}$$

$$\beta(\mathrm{x},\mathrm{t})=\sum_{m=1}^{\infty}\beta_m(t)\sin(\lambda x), \tag{57}$$

where $\lambda=m\pi/L$ and m is the half wave numbers in the x direction. Inserting the equations (41)-(57) into equations (41) to (44) and employing the Galerkin method, the following system of the algebraic equations can be obtained:

$$[M_m]\left[\ddot{\Delta}_m\right]+[C_m]\left[\dot{\Delta}_m\right]+\left([K]+N_m(t)\left[K_{pt}\right]\right)[\Delta_m]=0 \tag{58}$$

where dot indicates to derivative with respect to time and with the following definitions, $[K]$, $\left[K_{pt}\right]$ and $[M_m]$ are the stiffness, geometric stiffness and mass matrices, respectively

$$[M]=\begin{bmatrix} m_{11} & m_{12} & 0 & 0 & m_{15} \\ m_{21} & m_{22} & 0 & 0 & m_{25} \\ 0 & 0 & m_{33} & 0 & 0 \\ 0 & 0 & 0 & 0 & 0 \\ m_{51} & m_{52} & 0 & 0 & m_{55} \end{bmatrix}, \quad [\mathrm{K}]=\begin{bmatrix} k_{11} & k_{12} & 0 & k_{14} & k_{15} \\ k_{21} & k_{22} & k_{23} & k_{24} & m_{25} \\ 0 & k_{32} & k_{33} & k_{34} & k_{35} \\ k_{41} & k_{42} & k_{43} & k_{44} & k_{45} \\ k_{51} & k_{52} & k_{53} & k_{54} & k_{55} \end{bmatrix},$$
$$[C]=\begin{bmatrix} c_{11} & c_{12} & 0 & 0 & c_{15} \\ c_{21} & c_{22} & c_{23} & 0 & c_{25} \\ 0 & c_{32} & c_{33} & 0 & c_{35} \\ 0 & 0 & 0 & 0 & 0 \\ c_{51} & c_{52} & c_{53} & 0 & c_{55} \end{bmatrix}, \quad [K_{pt}]=\begin{bmatrix} 0 & 0 & 0 & 0 & 0 \\ 0 & 0 & 0 & 0 & 0 \\ 0 & 0 & k_{gg} & 0 & 0 \\ 0 & 0 & 0 & 0 & 0 \\ 0 & 0 & 0 & 0 & 0 \end{bmatrix}, \tag{59}$$

in which the components of mentioned matrices are shown in Appendix C.

Eq. (58) can be written in a reduced form to study static buckling analysis of the sandwich microbeam as follows [58]:

$$([K_t]+p_{cr}[K_{pt}])[\Delta_m]=0 \tag{60}$$

where p_{cr} is dimensionless critical buckling load of the structure.

4.1 Dynamic stability analysis

For dynamic stability analysis the periodic axial load is considered as [59]:

$$N_m(t)=p_{cr}\left[\alpha+\beta\cos(\Omega\,\mathrm{t})\right], \tag{61}$$

where α and β are the static and dynamic load factors, respectively. Also $\Omega=\omega L\sqrt{\rho/E}$ is dimensionless excitation frequency, in which ω is the excitation frequency.

By substituting Eq. (61) into Eq. (58) following relation can be obtained:

$$[M_m]\left[\ddot{\Delta}_m\right]+[C_m]\left[\dot{\Delta}_m\right]+\left([K_t]+p_{cr}\left[\alpha+\beta\cos(\Omega\,\mathrm{t})\right][K_{pt}]\right)[\Delta_m]=0 \tag{62}$$

According to this Bolotin method, the first instability region which is the most important region can be obtained by solving the following equation [58]:

$$\left|[K_t]-\alpha p_{cr}[K_{pt}]\pm\frac{\beta}{2}p_{cr}[K_{pt}]\mp\frac{\Omega}{2}[C]-\frac{\Omega^2}{4}[M_t]\right|=0. \tag{63}$$

where $|\;|$ indicates to determinant operator.

5 VERIFICATION

In order to verify the presented solution, a comparison is carried out for thermal dynamic stability analysis of sandwich microbeam of $h_{total} = 17.5\mu m$ with honeycomb core covered with piezoelectric and porous viscoelastic graphene face sheets. Material properties are considered as $E^c = 380 GPa, E_p = 70 GPa$, $\upsilon = 0.23$, $\rho_p = 3800 kg/m^3$ and $\rho_c = 2700 kg/m^3$. Table 1 shows the dimensionless deflection which are compared with those reported by Al shujairi and Mollamahmutoğlu [26]. This comparison confirms the high accuracy of he presented solution.

6 NUMERICAL RESULTS AND DISCUSSION

In this section, numerical results are provided for the presented solution. Results are presented in dimensionless form using following dimensionless parameters:

$$\begin{gathered}
(\bar{u}, \bar{w}, \theta, \varphi) = \left(\frac{u}{L}, \frac{w}{h_c}, \theta, \varphi\right), (\bar{x}, \bar{z}) = \left(\frac{x}{L}, \frac{z}{h_c}\right), \bar{t} = \frac{t}{L}\sqrt{\frac{E_m}{\rho_m}}, \bar{C}_{ij} = \frac{c_{ij}}{c_m}, \\
\bar{G}_{ij} = \frac{G_{ij}}{G_m}, \bar{E} = \frac{E.e_{31}}{E_m.h_m}, \mathrm{L}^* = \frac{L}{h_c}, \gamma = \frac{h_i}{h_c}, \bar{\mathrm{K}}_W = \frac{\mathrm{k_w} h_c}{E_m}, i^* = \frac{i}{h_c}, \mathrm{w}^* = \frac{w}{h_c} \\
\bar{\mathrm{K}}_G = \frac{\mathrm{k_G} h_c}{E_m}, \bar{e}_{ij} = \frac{e_{ij}}{e_{31}}, l^* = \frac{l}{h}, \Omega^* = \omega L\sqrt{\frac{\rho}{E}}, \bar{h}_{ij} = \frac{h_{ij} E_m}{e_{31}^2}, \bar{\mathrm{g}} = \frac{g}{L}\sqrt{\frac{E_m}{\rho_m}} \\
\bar{\mathrm{N}}_c = \frac{N_e}{E_c h_c}, \bar{\mathrm{N}}_T = \frac{N_T}{E_c h_c}, \bar{\rho}_{ij} = \frac{\rho_{ij}}{\rho_m}.
\end{gathered} \tag{64}$$

The material properties are considered to be temperature-dependent and for each mechhanical properties like P, following relation can be used [60]:

$$P(T) = C_0\left(C_{-1}T^{-1} + 1 + C_1 T + C_2 T^2 + C_3 T^3\right), \tag{65}$$

in which $T_1 = T_0 + \Delta T$ and $T_0 = 300K$ (room temperature) and C_0-C_3 are presented in Table 2. Also the material properties for the piezoelectric material are presented in Table 3.

In what follows, except for the cases which are mentioned directly, following values are considered: $h_t = h_c = h_b = 1\mu m$, L=10μm, $l_0 = l_1 = l_2 = 10^{-6}$, b=0.2 μm, ξ=0.4, ΔT=100 K.

The effect of the static load factor (α) on the instability regions of the sandwich microbeam is illustrated in Fig. 3. As depicted in this figure, with increase in the static load factor, the instability region of the sandwich microbeam tends to become wider and shifts to the coordinate origin which can be explained by decrease in total stiffness of the microbeam created by the static load.

The effect of slenderness ratio (length-to-thickness ratio) on the dynamic instability region of the sandwich microbeams is illustrated in Fig. 4. This figure shows that increase in the aspect ratio leads to lower excitation frequency. In addition, increase in length and decrease in thickness of the microbeam dramatically reduces the stiffness of microbeam.

Fig. 5. shows the dynamic instability regions of sandwich microbeams for different values of the temperature rise. According to this figure, it can be concluded that increase in the temperature moves the origins of the instability region to lower excitation frequency and decreases the width of the instability region of the sandwich microbeam at a certain values of dynamic load factor. For explain this conclusion, it should be noted that temperature rise generates a compressive axial load which reduces the stiffness of the microbeam.

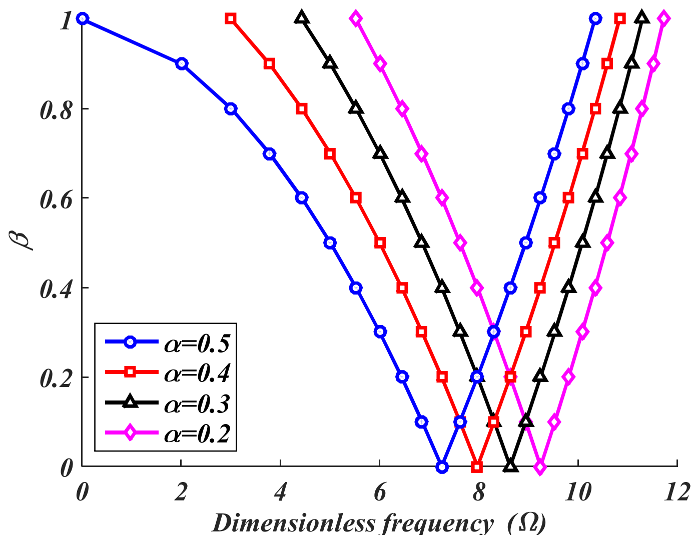

Fig. 3
Effect of static load factor on the instability region for sandwich microbeams.

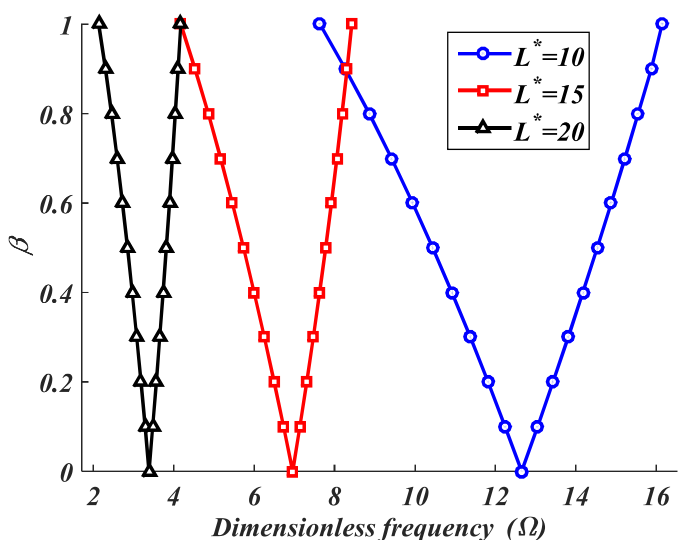

Fig. 4
Effect of beam aspect ratio on the instability region for a microbeam.

Fig. 6 is devoted to study the effect of small scale parameter on the instability region for sandwich microbeams. As shown in this figure, increase in value of small scale parameters moves the origins of the instability region to lower excitation frequency. It shows that small scale parameter has softening effect and increase in small scale parameter reduces the stiffness of the microbeam.

The influences of Winkler and Pasternak spring constants and viscoelastic coefficient of the foundation on the instability region for sandwich microbeams are depicted in Figs. 7-9. As shown in this figures, increase in the Winkler and Pasternak spring constants and viscoelastic coefficient of the foundation leads to higher excitation frequency and increase in the width of the instability region. It should be noticed that increasing in Winkler and Pasternak spring constants cause to increase the stiffness of foundation and increase in viscoelastic coefficient of the foundation leads to increase in damping of the foundation and stability of the microbeam.

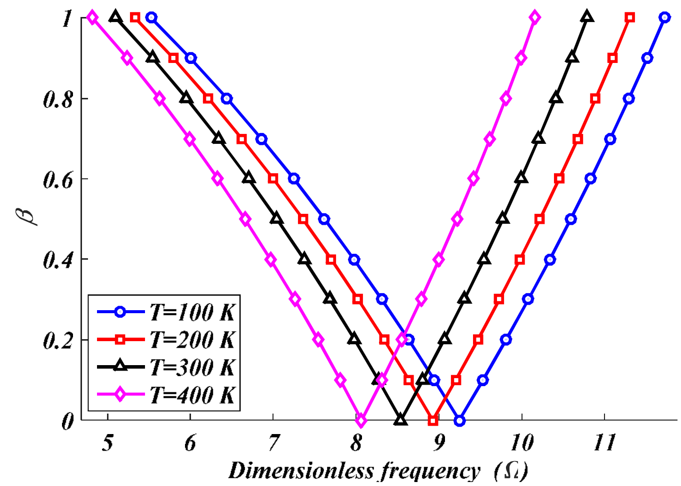

Fig. 5
Effect of temperature change on the instability region for sandwich microbeams.

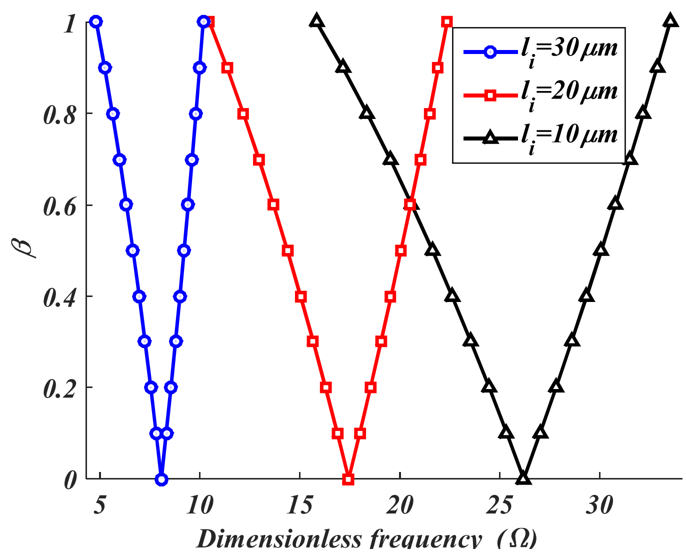

Fig. 6
Small scale effect on the instability region for sandwich microbeams.

Fig. 10. shows the effect of porosity index on the instability region for sandwich microbeams. As depicted in this figure, increase in the porosity index leads to reduction in excitation frequency which can be explained by reduction on stiffness of the microbeam created by increasing in size of pores.

The influence of visco porous graphene on the instability region for sandwich microbeams is shown in Fig. 11. As this figure shows, increase in the visco graphene reduces excitation frequency which can be explained by decrease in stiffness of the microbeam.

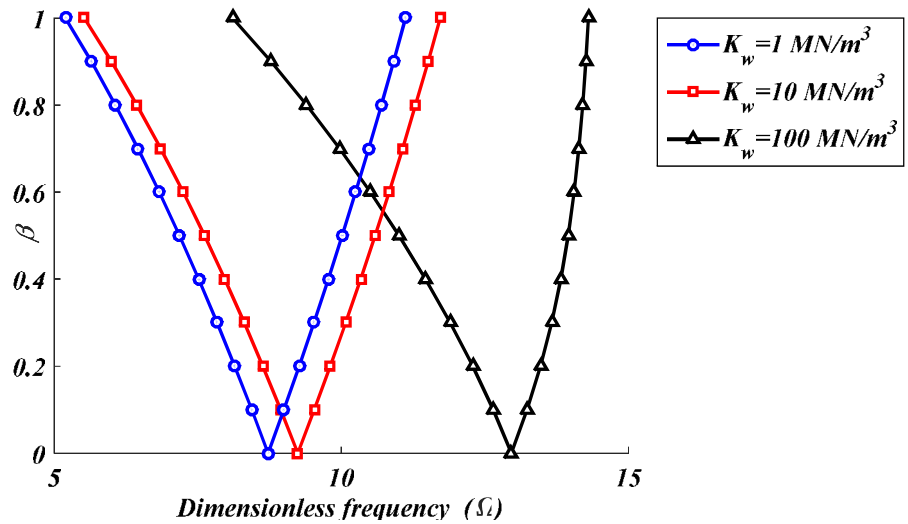

Fig. 7
Effect of Winkler spring constant of the foundation on the instability region for sandwich microbeams.

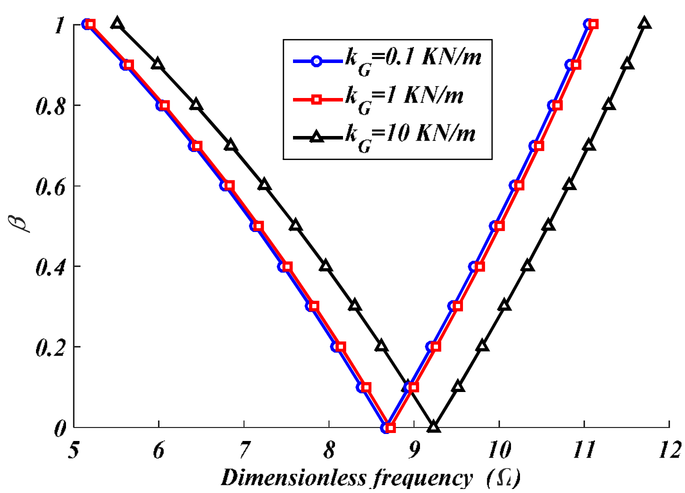

Fig. 8
Effect of Pasternak spring constant of the foundation on the instability region for sandwich microbeams.

Fig. 12. shows the dynamic instability region of a sandwich microbeam for different values of the electric load. As shown in this figure, positive values of the electric load move the origins of the instability regions to higher excitation frequency and increase the width of the instability region and negative values of the electric load have opposite effects. It is noteworthy that positive values of the electric load increase the stiffness of the microbeam and negative values of the electric load reduce the stiffness of the microbeam.

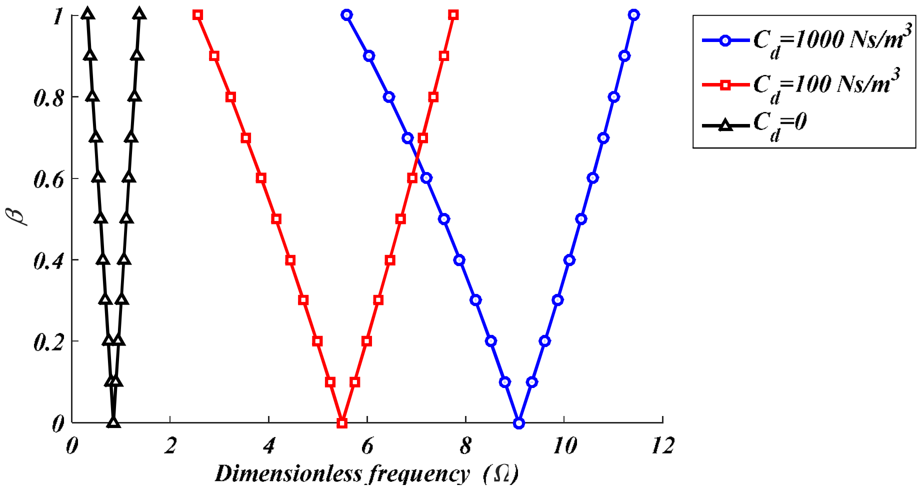

Fig. 9
Effect of viscoelastic coefficient of the foundation on the instability region for sandwich microbeams.

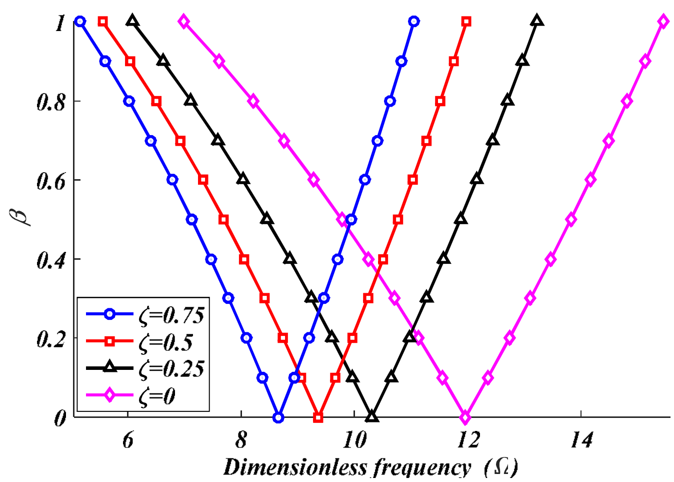

Fig. 10
Effect of porosity indexes on the instability region for sandwich microbeams.

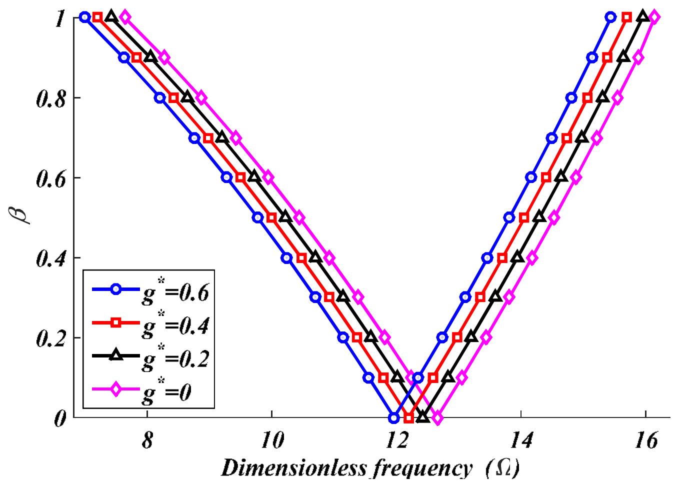

Fig. 11
Effect of visco porous graphene on the instability region for sandwich microbeams.

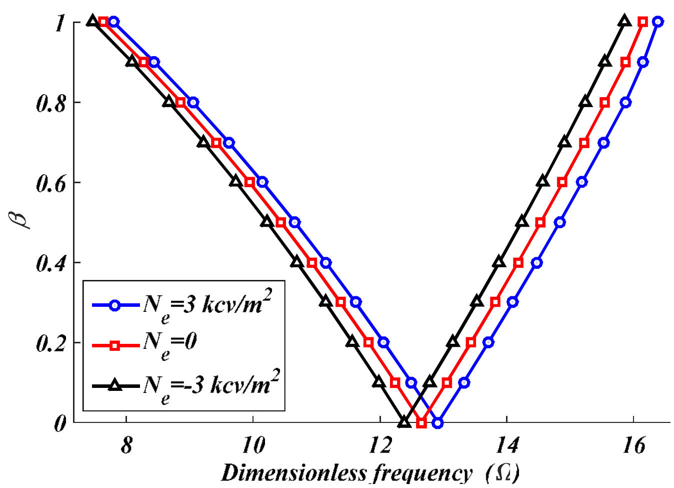

Fig. 12
Effect of versus electric load on the instability region for sandwich microbeams.

6 CONCLUSIONS

In this paper, thermal dynamic stability analysis of sandwich microbeam with honeycomb core and piezoelectric and porous viscoelastic graphene face sheets resting on visco Pasternak foundation was studied. The microbeam was modeled based on the zigzag beam theory. In order to consider the size effect, modified strain gradient theory was utilized and the set of the governing equations were derived using Hamilton's principle and were solved using Galerkin method. Using the presented numerical examples, the following conclusions can be drawn:

- ✓Increase in the static load factor, increase the width of the instability region of sandwich microbeams and shifts it closer to the coordinate origin.
- ✓Decrease in the effect of porosity indexes and visco graphene leads to increase in excitation frequency.
- ✓Increase in the Winkler spring constant and Pasternak medium leads to higher excitation frequency.
- ✓Increase in aspect ratio leads to lower excitation frequency.
- ✓Increase in temperature moves the origins of the instability regions to lower excitation frequency and decreases the width of the instability region of sandwich microbeam at a certain dynamic load factor.

✓Decrease in small scale parameters moves the origins of the instability regions to higher excitation frequencies.

APPENDIX A

$$\eta_{xxx}=\frac{\partial e_{xx}}{\partial x}-\frac{1}{5}\left(\frac{\partial e_{xx}}{\partial x}+2\frac{\partial e_{xx}}{\partial x}+\frac{\partial e_{xz}}{\partial z}\right)=\frac{2}{5}\frac{\partial^2 u}{\partial x^2}+\frac{2}{5}z\frac{\partial^2\theta}{\partial x^2}+\frac{2}{5}Q_1(z)\frac{\partial^2\psi}{\partial x^2}-\frac{2}{5}\frac{\mathrm{d}^2Q_1(z)}{\mathrm{d}z^2}\psi \tag{A-1}$$

$$\eta_{xxz}=\frac{1}{3}\left(2\frac{\partial e_{xz}}{\partial x}+\frac{\partial e_{xx}}{\partial z}\right)-\frac{1}{15}\left(\frac{\partial e_{xx}}{\partial z}+2\frac{\partial e_{xz}}{\partial z}\right)=\frac{8}{15}\frac{\partial^2 w}{\partial x^2}+\frac{4}{5}\frac{\partial\theta}{\partial x}+\frac{4}{5}\frac{\mathrm{d}Q_1(z)}{\mathrm{d}z}\frac{\partial\psi}{\partial x} \tag{A-2}$$

$$\eta_{xyy}=-\frac{1}{15}\left[\frac{\partial e_{xx}}{\partial x}+2\left(\frac{\partial e_{xx}}{\partial x}+\frac{\partial e_{xz}}{\partial z}\right)\right]=-\frac{1}{5}\frac{\partial^2 u}{\partial x^2}-\frac{1}{5}z\frac{\partial^2\theta}{\partial x^2}-\frac{1}{5}Q_1(z)\frac{\partial^2\psi}{\partial x^2}-\frac{2}{15}\frac{\mathrm{d}^2Q_1(z)}{\mathrm{d}z^2}\psi \tag{A-3}$$

$$\eta_{zzz}=-\frac{1}{5}\left(\frac{\partial e_{xx}}{\partial z}+2\frac{\partial e_{xz}}{\partial x}\right)=-\frac{2}{15}\frac{\partial^2 w}{\partial x^2}-\frac{1}{5}\frac{\partial\theta}{\partial x}-\frac{1}{5}\frac{\mathrm{d}Q_1(z)}{\mathrm{d}z}\frac{\partial\psi}{\partial x} \tag{A-4}$$

$$\eta_{xzz}=\frac{1}{3}\left(2\frac{\partial e_{xz}}{\partial z}\right)-\frac{1}{15}\left[\frac{\partial e_{xx}}{\partial x}+2\left(\frac{\partial e_{xx}}{\partial x}+\frac{\partial e_{xz}}{\partial z}\right)\right]=\frac{8}{15}\frac{\mathrm{d}^2Q_1(z)}{\mathrm{d}z^2}\psi-\frac{1}{5}\frac{\partial^2 u}{\partial x^2}-\frac{1}{5}z\frac{\partial^2\theta}{\partial x^2}-\frac{1}{5}Q_1(z)\frac{\partial^2\psi}{\partial x^2} \tag{A-5}$$

$$\eta_{yyz}=-\frac{1}{15}\left(\frac{\partial e_{xx}}{\partial z}+2\frac{\partial e_{xz}}{\partial x}\right)=-\frac{2}{5}\frac{\partial^2 w}{\partial x^2}-\frac{3}{5}\frac{\partial\theta}{\partial x}-\frac{3}{5}\frac{\mathrm{d}Q_1(z)}{\mathrm{d}z}\frac{\partial\psi}{\partial x} \tag{A-6}$$

$$\tau_{xxx}=2l_1^2G\eta_{xxx} \tag{A-7}$$

$$\tau_{xyy}=2l_1^2G\eta_{xyy} \tag{A-8}$$

$$\tau_{xxz}=2l_1^2G\eta_{xxz} \tag{A-9}$$

$$\tau_{xzz}=2l_1^2G\eta_{zzx} \tag{A-10}$$

$$\tau_{yyz}=2l_1^2G\eta_{yyz} \tag{A-11}$$

$$\tau_{zzz}=2l_1^2G\eta_{zzz} \tag{A-12}$$

$$p_x=2l_0^2G\gamma_x \tag{A-13}$$

$$p_z=2l_0^2G\gamma_z \tag{A-14}$$

$$\chi_{xy}=\frac{1}{2}\left(-\frac{1}{2}\frac{\partial\gamma_{xz}}{\partial x}+\frac{\partial e_{xx}}{\partial z}\right)=-\frac{1}{4}\frac{\partial^2 w}{\partial x^2}+\frac{1}{4}\frac{\partial\theta}{\partial x}+\frac{1}{4}\frac{\mathrm{d}Q_1(z)}{\mathrm{d}z}\frac{\partial\psi}{\partial x} \tag{A-15}$$

$$\chi_{yz}=\frac{1}{2}\left(\frac{1}{2}\frac{\partial\gamma_{xz}}{\partial z}\right)=\frac{1}{4}\frac{\mathrm{d}^2Q_1(z)}{\mathrm{d}z^2}\psi \tag{A-16}$$

$$m_{xy}=2l_2^2G\chi_{xy} \tag{A-17}$$

$$m_{xy}=2l_2^2G\chi_{xy} \tag{A-18}$$

$$m_{yz}=2l_2^2G\chi_{yz} \tag{A-19}$$

$$\gamma_x=\frac{\partial e_{xx}}{\partial x}=\frac{\partial^2 u}{\partial x^2}+z\frac{\partial^2\theta}{\partial x^2}+Q_1(z)\frac{\partial^2\psi}{\partial x^2} \tag{A-20}$$

$$\gamma_z=\frac{\partial e_{zz}}{\partial z}=\frac{\partial\theta}{\partial x}+\frac{\mathrm{d}Q_1(z)}{\mathrm{d}z}\frac{\partial\psi}{\partial x} \tag{A-21}$$

APPENDIX B

$$I_0=\int dz \tag{B-1}$$

$$I_1=\int zdz \tag{B-2}$$

$$I_2=\int z^2dz \tag{B-3}$$

$$I_3=\int \rho_c(z)dz \tag{B-4}$$

$$I_4=\int z\rho_c(z)dz \tag{B-5}$$

$$I_5=\int Q_1(z)\rho_c(z)dz \tag{B-6}$$

$$I_6=\int Q_1^2(z)\rho_c(z)dz \tag{B-7}$$

$$I_7=\int C_{11}(z)dz \tag{B-8}$$

$$I_8=\int Q_1(z)dz \tag{B-9}$$

$$I_9=\int C_{55}(z)dz \tag{B-10}$$

$$I_{10}=\int\left[\frac{dQ_1(z)}{dz}\right]^2 dz \tag{B-11}$$

$$I_{11}=\int\left[\frac{d^2Q_1(z)}{dz^2}\right]^2 dz \tag{B-12}$$

$$I_{12}=\int Q_1^2(z)\,dz \tag{B-13}$$

$$I_{13}=\int \frac{dQ_1(z)}{dz}dz \tag{B-14}$$

$$I_{14}=\int \frac{d^2Q_1(z)}{dz^2}dz \tag{B-15}$$

$$I_{15}=\int \sin\left(\frac{\pi\bar{z}}{h_i}\right)dz \qquad i=e,\mathrm{m} \tag{B-16}$$

$$I_{16}=\int \sin^2\left(\frac{\pi\bar{z}}{h_i}\right)dz \qquad i=e,\mathrm{m} \tag{B-17}$$

$$I_{17}=\int \cos\left(\frac{\pi}{h_i}\bar{z}\right)dz \qquad i=e,m \tag{B-18}$$

$$I_{18}=\int \cos^2\left(\frac{\pi\bar{z}}{h_i}\right)dz \qquad i=e,m \tag{B-19}$$

APPENDIX C

$$k_{11}=\left(\frac{C_{11}I_{0c}}{E_cL}+\frac{C_{11}I_{0e}}{E_cL}+\frac{C_{11}I_{19g}}{E_cL}\right)\lambda^2+\left(\frac{C_{55j}i_1^2I_{0j}}{E_cL^3}+\frac{4C_{55j}i_1^2I_{0j}}{5E_cL^3}\right)\lambda^4 \tag{C-1}$$

$$k_{12}=\left(\frac{C_{11}I_{1c}}{E_cL^2}+\frac{C_{11}I_{1e}}{E_cL^2}+\frac{C_{11}I_{14g}}{E_cL^2}\right)\lambda^2+\left(\frac{2C_{55j}i_0^2I_{1j}}{E_cL^4}+\frac{4C_{55j}i_1^2I_{1j}}{5E_cL^4}\right)\lambda^4 \tag{C--2}$$

$$k_{13}=0 \tag{C-3}$$

$$k_{14}=-\frac{\pi I_{29e}}{L}\lambda \tag{C-4}$$

$$k_{15}=\left(\frac{C_{11}I_{3e}}{E_cL^2}+\frac{4C_{55j}i_1^2I_{22j}}{5E_cL^2}+\frac{I_{15g}}{E_cL^2}\right)\lambda^2+\left(\frac{4C_{55j}i_1^2I_{9j}}{5E_cL^4}+\frac{2C_{55j}i_0^2I_{9j}}{E_cL^4}\right)\lambda^4 \tag{C-5}$$

$$k_{21}=\left(\frac{C_{11}I_{1c}}{E_ch_cL}+\frac{C_{11}I_{1e}}{E_ch_cL}+\frac{I_{14g}}{E_ch_cL}\right)\lambda^2+\left(\frac{2C_{55j}i_0^2I_{1j}}{5E_cL^3h_c}+\frac{4C_{55j}i_1^2I_{1j}}{5E_cL^3h_c}\right)\lambda^4 \tag{C-6}$$

$$\begin{aligned}k_{22}&=\frac{k_sC_{55c}I_{0c}}{E_ch_c}+\frac{k_sI_{12g}}{E_ch_c}+\frac{k_sC_{55e}I_{0c}}{E_ch_c}+\left(\frac{4C_{55j}i_1^2I_{2j}}{E_cL^4}+\frac{2C_{55j}i_0^2I_{2j}}{5E_cL^3h_c}\right)\lambda^4\\&+\left(\frac{C_{11}I_{2c}}{E_ch_cL^2}+\frac{C_{11}I_{2e}}{E_ch_cL^2}+\frac{C_{55j}i_2^2I_{0j}}{8E_cL^2h_c}+\frac{2C_{55j}i_0^2I_{0j}}{5E_cL^2h_c}+\frac{24C_{55j}i_1^2I_{0j}}{5E_cL^2h_c}+\frac{k_sC_{55c}I_{11g}}{E_cL}+\frac{C_{11}I_{16g}}{E_ch_cL^2}\right)\lambda^2\end{aligned} \tag{C-7}$$

$$k_{23}=\left(\frac{k_sC_{55e}I_{0c}}{E_cL}+\frac{k_sC_{55e}I_{0c}}{E_cL}+\frac{k_sC_{55e}I_{12g}}{E_cL}\right)\lambda+\left(\frac{24C_{55j}i_1^2I_{0j}}{5E_cL^2h_c}-\frac{C_{55j}i_2^2I_{0j}}{8E_cL^3}\right)\lambda^3 \tag{C-8}$$

$$k_{24}=-\frac{\pi I_{30e}}{E_cL}\lambda \tag{C-9}$$

$$\begin{aligned}k_{25}&=\frac{k_sC_{55e}I_{11e}}{E_ch_cL^2}+\frac{k_sI_{18g}}{E_cL}+\frac{I_{5g}}{\rho_cL^2}+\left(\frac{4C_{55j}i_1^2I_{26j}}{5E_cL^4h_c}+\frac{2C_{55j}i_0^2I_{26j}}{5E_cL^4h_c}\right)\lambda^4\\&+\left(\frac{C_{11e}I_{26e}}{E_ch_cL^2}+\frac{2C_{55j}i_0^2I_{11j}}{5E_cL^2h_c}+\frac{2C_{55j}i_1^2I_{24j}}{5E_cL^2h_c}+\frac{I_{13g}}{E_ch_cL^2}+\frac{C_{55j}i_2^2I_{22j}}{8E_ch_c}+\frac{24C_{55j}i_0^2I_{11j}}{5E_cL^2h_c}\right)\lambda^2\end{aligned} \tag{C-10}$$

$$k_{31}=0 \tag{C-11}$$

$$k_{32}=\left(\frac{k_sC_{55c}I_{0c}}{E_cL}+\frac{k_sC_{55e}I_{0e}}{E_ch_c}+\frac{k_sI_{12g}}{E_cL}\right)\lambda+\left(\frac{16C_{55j}i_0^2I_{0j}}{5E_cL^3}-\frac{C_{55j}i_2^2I_{0j}}{8E_cL^3}\right)\lambda^3 \tag{C-12}$$

$$\begin{aligned}k_{33}&=-\frac{k_wh_c}{E_c}+\left(\frac{k_sC_{55c}h_cI_{0c}}{E_cL^2}-\frac{k_G}{E_cL}-\frac{N^Th_c}{E_cL^2}-\frac{N_xh_c}{E_cL^2}+\frac{k_sC_{55e}h_cI_{0e}}{E_cL^2}+\frac{k_sh_cI_{12g}}{E_cL^2}\right)\lambda^2\\&+\left(\frac{C_{55j}h_ci_2^2I_{0j}}{8E_cL^4}+\frac{C_{55j}i_2^2I_{0j}}{8E_cL^3}\right)\lambda^4\end{aligned} \tag{C-13}$$

$$k_{34}=0 \tag{C-14}$$

$$k_{35}=\left(\frac{C_{55e}k_sI_{11e}}{E_cL}+\frac{C_{55c}k_sI_{11c}}{E_cL}+\frac{k_sI_{18g}}{E_cL}\right)\lambda-\left(\frac{C_{55j}i_2^2I_{11j}}{8E_cL^3}+\frac{16C_{55j}i_0^2I_{11j}}{5E_cL^3}\right)\lambda^3 \tag{C-15}$$

$$k_{41}=-\frac{\pi I_{29e}}{h_c}\lambda \tag{C-16}$$

$$k_{42}=-\frac{\pi I_{30e}}{Lh_c}\lambda \tag{C-17}$$

$$k_{43}=0 \tag{C-18}$$

$$k_{44}=-\frac{Eh_ch_{33}I_{29e}}{h_e^2e_{31}^2}-\frac{Eh_ch_{11}I_{27e}}{e_{31}^2L^2}\lambda^2 \tag{C-19}$$

$$k_{45}=-\frac{\pi e_{31}I_{33e}}{h_c}\lambda \tag{C-20}$$

$$k_{51}=\left(\frac{C_{11}I_{9e}}{E_cLh_c}+\frac{4C_{55j}i_0^2I_{22j}}{5E_cLh_c}+\frac{I_{15g}}{E_cL}\right)\lambda^2+\left(\frac{2C_{55j}i_0^2I_{9j}}{5E_cL^3h_c}+\frac{4C_{55j}i_1^2I_{1j}}{5E_cL^3h_c}\right)\lambda^4 \tag{C-21}$$

$$\begin{aligned}k_{52}=&\frac{k_sI_{18g}}{E_cL}+\frac{k_sC_{55e}I_{11e}}{E_ch_c}\lambda+\left(\frac{4C_{55j}i_1^2I_{26j}}{5E_cLh_c}+\frac{2C_{55j}i_0^2I_{26j}}{E_cL^4h_c}\right)\lambda^4\\&+\left(\frac{C_{11e}I_{26e}}{E_cL^2h_c}+\frac{I_{13g}}{E_cL^2h_c}+\frac{2C_{55j}i_0^2I_{11j}}{E_cL^2h_c}+\frac{24C_{55j}i_1^2I_{11j}}{5E_cL^2h_c}+\frac{4C_{55j}i_1^2I_{24j}}{5E_cL^2h_c}+\frac{C_{55j}i_2^2I_{11j}}{8E_cL^2h_c}\right)\lambda^2\end{aligned} \tag{C-22}$$

$$k_{53}=\left(\frac{k_sI_{18g}}{E_cL}+\frac{k_sC_{55e}I_{11e}}{E_cL}+\frac{k_sC_{55c}I_{11c}}{E_cL}+\frac{k_sC_{55c}I_{11c}}{E_cL}\right)\lambda+\left(\frac{16C_{55j}i_1^2I_{11j}}{5E_cL^3}-\frac{C_{55j}i_2^2I_{11j}}{8E_cL^3h_c}\right)\lambda^3 \tag{C-23}$$

$$k_{54}=-\frac{\pi I_{33e}}{h_eL}\lambda \tag{C-24}$$

$$\begin{aligned}k_{55}=&\frac{C_{11e}I_{26e}}{E_ch_cL^2}-\frac{k_sC_{55c}I_{20c}}{E_ch_c}+\frac{k_sI_{21e}}{E_ch_c}+\frac{k_sC_{55c}I_{20c}}{E_ch_c}+\left(\frac{4C_{55j}i_1^2I_{23j}}{5E_cL^4h_c}+\frac{2C_{55j}i_0^2I_{23j}}{5E_cL^4h_c}\right)\lambda^4\\&+\left(\frac{C_{11e}I_{23e}}{E_ch_cL^2}+\frac{8C_{55j}i_1^2I_{25j}}{5E_cL^2h_c}+\frac{24C_{55j}i_1^2I_{20j}}{5E_cL^2h_c}+\frac{2C_{55j}i_0^2I_{20j}}{5E_cL^2h_c}+\frac{C_{55j}i_2^2I_{20j}}{8E_cL^2h_c}+\frac{I_{17g}}{E_ch_cL^2}+\frac{I_{7g}}{\rho_ch_cL^2}\right)\lambda^2\end{aligned} \tag{C-25}$$

$$m_{11}=\frac{I_{0c}}{L}+\frac{I_{0e}\rho_e}{L\rho_c}+\frac{I_{3g}}{L\rho_c} \tag{C-26}$$

$$m_{12}=\frac{I_{1c}}{L^2}+\frac{I_{1e}\rho_e}{L^2\rho_c}+\frac{I_{4g}}{L^2\rho_c} \tag{C-27}$$

$$m_{15}=\frac{I_{9e}\rho_e}{L^2\rho_c}+\frac{I_{5g}}{L^2\rho_c}-\frac{I_{9c}}{L^2} \tag{C-28}$$

$$m_{21}=\frac{I_{1c}}{Lh_c}+\frac{I_{2e}\rho_e}{h_cL^2\rho_c}+\frac{I_{4g}\rho_e}{h_cL\rho_c} \tag{C-29}$$

$$m22 = \frac{I_{2c}}{L^2 h_c} + \frac{I_{2e}\rho_e}{L^2 h_c \rho_c} + \frac{I_{6g}}{L^2 h_c \rho_c} A_{10} \tag{C-30}$$

$$m_{51} = \frac{I_{9e}}{Lh_c} + \frac{I_{5e}}{L\ \rho_c h_c} - \frac{I_{9c}}{L\ h_c} \tag{C-31}$$

$$m_{52} = \frac{I_{26e}}{L^2 h_c} + \frac{I_{7g}}{h_c L^2 \rho_c} + \frac{I_{9C}}{L\ h_c} \tag{C-32}$$

$$m_{55} = \frac{I_{23e}\rho_e}{L^2 \rho_c h_c} + \frac{I_{8g}}{L^2 h_c \rho_c} + \frac{I_{23c}}{L^2 h_c} \tag{C-33}$$

$$C_{11} = \frac{I_{19g}\overline{g}}{L\ E_c}\lambda^2 \tag{C-34}$$

$$C_{12} = \frac{I_{14g}\overline{g}}{L^2 E_c}\lambda^2 \tag{C-35}$$

$$C_{15} = \frac{I_{15g}\overline{g}}{L^2 E_c}\lambda^2 \tag{C-36}$$

$$C_{21} = \frac{I_{14g}\overline{g}}{h_c L\ E_c}\lambda^2 \tag{C-37}$$

$$C_{22} = \frac{k_s I_{12g}\overline{g}}{h_c E_c} + \left(\frac{I_{16g}\overline{g}}{h_c L^2 E_c} + \frac{I_{16g}\overline{g}}{h_c L^2 E_c}\right)\lambda^2 \tag{C-38}$$

$$C_{23} = \frac{k_s I_{12g}\overline{g}}{LE_c}\lambda \tag{C-39}$$

$$C_{25} = \frac{k_s I_{13g}\overline{g}}{h_c L^2 E_c} + \frac{I_{13g}\overline{g}}{h_c L^2 E_c}\lambda^2 \tag{C-40}$$

$$C_{32} = \frac{k_s I_{12g}\overline{g}}{h_c L}\lambda \tag{C-41}$$

$$C_{33} = -\frac{C_d h_c}{L^2\sqrt{E_c \rho_c}} + \frac{k_s I_{12g} h_c \overline{g}}{E_c L^2}\lambda^2 \tag{C-42}$$

$$C_{35} = \frac{k_s I_{18g}\overline{g}}{E_c L}\lambda \tag{C-43}$$

$$C_{51} = \frac{I_{15g}\overline{g}}{h_c E_c L}\lambda^2 \quad \text{(C-44)}$$

$$C_{52} = \frac{I_{13g}\overline{g}}{h_c E_c L^2}\lambda^2 + \frac{k_s I_{18g}\overline{g}}{h_c E_c} \quad \text{(C-45)}$$

$$C_{53} = \frac{k_s I_{18g}\overline{g}}{L E_c}\lambda \quad \text{(C-46)}$$

$$C_{55} = \frac{k_s I_{21g}\overline{g}}{h_c E_c} + \frac{I_{17g}\overline{g}}{h_c L^2 E_c}\lambda^2 \quad \text{(C-48)}$$

$$k_{gg} = \lambda^2 \quad \text{(C-49)}$$

REFERENCES

[1] Salvetat-Delmotte JP, Rubio A, 2002, Mechanical properties of carbon nanotubes: a fiber digest forbeginners, *Carbon* , 40(10):1729-1734.

[2] Esawi AMK, Farag MM, 2007, Carbon nanotube reinforced composites: potential and current challenges, *Material Design*, 28(9):2394-2401.

[3] Fiedler B, Gojny FH, Wichmann MHG, Nolte MCM, Schulte K, 2006, Fundamental aspects of nano-reinforced composites. *Composite Science and Technology*; 66:3115-3125.

[4] Mohammadimehr M, Monajemi A.A, Afshari H, 2020, Free and forced vibration analysis of viscoelastic damped FG-CNT reinforced micro composite beams, *Microsystem Technologies*, 26: 3085–3099.

[5] Mohammadimehr M, Mohammadi Hooyeh H, Afshari H, Salarkia M.R., 2016, Size-dependent Effects on the Vibration Behavior of a Timoshenko Microbeam subjected to Pre-stress Loading based on DQM, *Mechanics of Advanced Composite Structures*, 3: 99-112.

[6] Mohammadimehr M, Emdadi M, Afshari H, Rousta Navi B, 2018, Bending, buckling and vibration analyses of MSGT microcomposite circular-annular sandwich plate under hydro-thermo-magneto-mechanical loadings using DQM, International *Journal of Smart and Nano Materials*, 9(4).

[7] Afshari, H. and Adab N, 2020. Size-dependent buckling and vibration analyses of GNP reinforced microplates based on the quasi-3D sinusoidal shear deformation theory. *Mechanics Based Design of Structures and Machines*, In Press.

[8] Zheng S, Chen M, Li Z, and Wang H, 2016, Size-dependent constituent equations of piezoelectric bimorphs, *Composite Structures,* 150: 1–7.

[9] Zheng S, Li Z, Chen M, and Wang H, 2016, Size-dependent static bending and free vibration of polarized PLZT micro cantilevers, *Smart Mater. Structures,* 28(20):2920-2932.

[10] Chen M and Zheng S, 2017, Size-dependent static bending of a microbeam with a surface-mounted 0–1 polarized PbLaZrTi actuator under various boundary conditions, *Material Systems and Structures*, 28: (20): 2920-2932.

[11] Nejati M, Ghasemi A-, Soltanimaleki A, Dimitri R, Tornabene F, 2019, Thermal vibration analysis of SMA hybrid composite double curved sandwich panels, *Composite Structures*, 224:111035.

[12] Arshid E, Khorshidvand A.R, 2018, Free vibration analysis of saturated porous FG circular plates integrated with piezoelectric actuators via differential quadrature method, *Thin-Walled Structures*, 125: 220-233.

[13] Arshid E, Amir S, Loghman A, 2020, Static and dynamic analyses of FG-GNPs reinforced porous nanocomposite annular micro-plates based on MSGT, *International Journal of Mechanical Sciences*, 180:105656.

[14] Kiani A, Amir S, Zarghami Dehaghani M, 2019, Asymmetric free vibration analysis of first-order shear deformable functionally graded magneto-electro-thermo-elastic circular plates, *Journal of Mechanical Engineering Science*, 233: 5659-5675.

[15] Mohammadimehr M, Arshid E, Alhosseini S.M.A, Amir S, Arani Ghorbanpour M. R, 2019, Free vibration analysis of thick cylindrical MEE composite shells reinforced CNTs with temperature-dependent properties resting on viscoelastic foundation, *Structural Engineering and Mechanics*, 70: 683-702.

[16] Arshid E, Kiani A, Amir S, 2019, Magneto-electro-elastic vibration of moderately thick FG annular plates subjected to multi physical loads in thermal environment using GDQ method by considering neutral surface, *Journal of Materials: Design and Applications*, 233: 2140-2159.

[17] Amine Daikh A, Ashraf M. Zenkour A.M, 2019, Effect of porosity on the bending analysis of various functionally gradedsandwich plates, *Materials Research Express*.
[18] Amir S, Soleimani Z, Arshid E, 2019, Size□dependent free vibration of sandwich micro beam with porous core subjected to thermal load based on SSDBT, 99: e201800334.
[19] Amir S, Arshid E, Alhosseini S. M. A, Loghman A, 2019, Quasi-3D tangential shear deformation theory for size-dependent free vibration analysis of three-layered FG porous micro rectangular plate integrated by nano-composite faces in hygrothermal environment, *Journal of Thermal Stresses*, 43: 133-156.
[20] Amir S, Arshid E, Ghorbanpour Arani M.R, 2019, Size-dependent magneto-electro-elastic vibration analysis of FG saturated porous annular/ circular micro sandwich plates embedded with nano-composite face sheets subjected to multi-physical pre loads, *Smart Structures and Systems*, 23: 429-447.
[21] Amir S, Vossough A.R, Vossough H, Arshid E, 2020, Nonlinear Magneto-Nonlocal Vibration Analysis of Coupled Piezoelectric Micro-Plates Reinforced with Agglomerated CNTs, *Mechanics of Advanced Composite Structures*, 7: 109-119.
[22] Amir S, Khorasani M, BabaAkbar-Zarei H, 2020, Buckling analysis of nanocomposite sandwich plates with piezoelectric face sheets based on flexoelectricity and first-order shear deformation theory, *Journal of Sandwich Structures & Materials*, 22: 2186-2209.
[23] Amir S, Rezaei Bidgoli E.M, Arshid E, 2020, Size-dependent vibration analysis of a three-layered porous rectangular nano plate with piezo-electromagnetic face sheets subjected to pre loads based on SSDT, *Mechanics of Advanced Materials and Structures*, 27: 605-619.
[24] Karami B, Janghorban M, Shahsavari D, Dimitri R, Tornabene F, 2019, Nonlocal Buckling Analysis of Composite Curved Beams Reinforced with Functionally Graded Carbon Nanotubes, *Molecules*, 24:2750.
[25] Yoosefian A.R, Golmakani M.E, Sadeghian M, 2020, Nonlinear bending of functionally graded sandwich plates under mechanical and thermal load, Journal Pre-proof, 84:105-161.
[26] Al Shujairi M., Mollamahmutoglu Ç, 2018, investigated Buckling and free vibration analysis of functionally graded sandwich micro-beams resting on elastic foundation by using nonlocal strain gradient theory in conjunction with higher order shear theories under thermal effect, *Composites Part B,* 154:292-312.
[27] Aria A.I, Friswell M.I, 2019, Computational hygro-thermal vibration and buckling analysis of functionally graded sandwich microbeams, *Composites Part B* 165: 785–797.
[28] Chen Z, Li J, Sun L, Li L, 2019, Flexural buckling of sandwich beams with thermal-induced non-uniform sectional properties, *Journal of Building Engineering* 25: 100782.
[29] Esen I, 2019, Dynamic response of functional graded Timoshenko beams in a thermal environment subjected to an accelerating load, *European Journal of Mechanics / A Solids*, 78: 10384.
[30] Ghorbanpour Arani A, Zarei H.B, Pourmousa P, Eskandari M, 2018, Investigation of free vibration response of smart sandwich micro-beam on Winkler–Pasternak substrate exposed to multi physical fields, *Microsystem Technologies*, 24:3045–3060.
[31] Fu T, Chen Z, Yu H, Li Ch, Zhao Y, 2019, Thermal buckling and sound radiation behavior of truss core sandwich panel resting on elastic foundation, *International Journal of Mechanical Sciences* 161: 105055.
[32] Yuan W, Wang X, Song H.W, Huang C.G, 2014, A theoretical analysis on the thermal buckling behavior of fully clamped sandwich panels with truss cores. *J Therm Stress*, 37(12):1433–48.
[33] W Yuan, HW Song, Huang CG, 2016, Failure maps and optimal design of metallic sandwich panels with truss cores subjected to thermal loading. *Int J Mech Sci*, 115:56–67.
[34] Mohammadimehr M, Mohammadi Hooyeh M, Afshari H, Salarkia M.R., 2016, Free vibration analysis of double-bonded isotropic piezoelectric Timoshenko micro-beam based on strain gradient and surface stress elasticity theories under initial stress using DQM, *Mechanics of Advanced Materials and Structures*, 24(6).
[35] Torabi K, Afshari H, Aboutalebi F.H., Vibration and flutter analyses of cantilever trapezoidal honeycomb sandwich plates, *Journal of Sandwich Structures & Materials*, 21(8): 2887-2920.
[36] Li Ch, Shen H, Wang H, 2019, Thermal post-buckling of sandwich beams with functionally graded negative Poisson's ratio honeycomb core, *International Journal of Mechanical Sciences* 152: 289–297.
[37] Liu Y, Shengkai Su, Huang H, Liang Y, 2018, Thermal-mechanical coupling buckling analysis of porous functionally graded sandwich beams based on physical neutral plane, *Composites Part B, 168:236-242.*
[38] Marynowski K, 2018, Vibration analysis of an axially moving sandwich beam with multiscale composite facings in thermal environment, *International Journal of Mechanical Sciences* 146: 116–124.
[39] Pradhan M, Dash P.R, 2016, Stability of An Asymmetric Tapered Sandwich Beam Resting On A Variable Pasternak Foundation Subjected To A Pulsating Axial Load With Thermal Gradient, *Composite Structures*, 140 : 816-834.
[40] Waddar S, Pitchaimani J, Doddamani M, Barbero E, 2019, Buckling and vibration behaviour of syntactic foam core sandwich beam with natural fiber composite facings under axial compressive loads, *Composites Part B*, 175:107133.
[41] Carrera E, 2003, Historical review of zigzag theories for multilayered plate and shell, *Mech. Rev*, 56:287–308.
[42] Tessler.A, Sciuva M Di, Gherlone M, 2009, A refined zigzag beam theory for composite and sandwich beams, *Journal of composite*, 43: 1051-1081.
[43] Ghorbanpour Arani A, Kolahchi R, Vossough H, 2013, Buckling analysis and smart control of SLGS using elastically coupled PVDF nanoplate based on nonlocal Mindlin plate theory, 407: 4458-4465.

[44] He X Q, Ng T.Y, Sivashanker S, Liew K.M, 2001, Active control of FGM plates with integrated piezoelectric sensors and actuators, *International Journal of Solids and Structures* 38: 1641-1655.
[45] Ke LL, Liu C, Wang YS, 2015, Free vibration of nonlocal piezoelectric nanoplates under various boundary conditions. *Phys E*, 66:93–106.
[46] Chen D, Yang J and Kitipornchai S, 2015, Elastic buckling and static bending of shear deformable functionally graded porous beam. *Compos Structures*, 133: 54–61.
[47] Al Rjoub YS and Hamad AG, 2017, Free vibration of functionally Euler-Bernoulli and Timoshenko graded porous beams using the transfer matrix method. *KSCE J Civ Eng*, 21: 792–806.
[48] Shafiei N, Mousavi A and Ghadiri M, 2016, On size-dependent nonlinear vibration of porous and imperfect functionally graded tapered microbeams. *Int J Eng Sci*, 106: 42–56.
[49] Hong C.C, 2014, Thermal vibration and transient response of magnetostrictive functionally graded material plates, European *Journal of Mechanics A/Solids*, 43: 78-88.
[50] Kandasamy R , Dominique S, 2018, Finite Element Based Active Vibration Control of Hierarchical Honeycomb Plates Integrated with Piezoelectric Actuator, *SAE International*, https://doi.org/10.4271/2018-01-1558.
[51] An L.Q., Zhang X.C., Wu H.X., Jiang W.Q, 2017, In-PlaneDynamic Crushing and Energy Absorption Capacity of SelfSimilar Hierarchical Honeycombs, *Advances in Mechanical Engineering,* 9(6):1-15.
[52] Mousanezhad D. Haghpanah B, Ghosh R., Hamouda A.M, 2016, Elastic Properties of Chiral, Anti-Chiral, and Hierarchical Honeycombs: A Simple Energy-Based Approach, *Theoretical and Applied Mechanics Letters* 6(2):81-96.
[53] Su Z, Jin G, Wang Y, Ye X, 2016, A general Fourier formulation for vibration analysis of functionally graded sandwich beams with arbitrary boundary condition and resting on elastic foundations, *Acta Mech*, 227(5):1493–1514.
[54] Ghorbanpour Arani A, Amir S, 2013, Electro-thermal vibration of visco-elastically coupled BNNT systems conveying fluid embedded on elastic foundation via strain gradient theory, *Physica B*, 419:1–6.
[55] Mohammadimehr M, Mohammadi Hooyeh H, Afshari H, Salarkia M.R, 2016, Size-dependent Effects on the Vibration Behavior of a Ti-moshenko Microbeam subjected to Pre-stress Loading based on DQM, *Mechanics of Advanced Composite Structures*, 3:99-112.
[56] Kolahchi R, Dynamic stability analysis of temperature-dependent functionally graded CNT reinforced visco-plates resting on orthotropic elastomeric medium.
[57] Ansari R, Gholami R, Sahmani S, 2012, On the dynamic stability of embedded single-walled carbon nanotubes including thermal environment effects, *Scientia Iranica* F, 19 (3):919–925.
[58] Saffari SH, Hashemian M, Toghraie D, 2017, Dynamic stability of functionally graded nanobeam based on nonlocal Timoshenko theory considering surface effects, http://dx.doi.org/10.1016/j.physb.2017.06.029.
[59] He X.Q., Ng T.Y, Sivashanker S, Liew K.M, 2001, Active control of FGM plates with integrated piezoelectric sensors and actuators, *International Journal of Solids and Structures*, 38: 1641-1655.
[60] Lam K.Y., Ng T.Y, 1999, Active control of composite plates with integrated piezoelectric sensors and actuators under various dynamic loading conditions. *Smart Materials and Structures*, 8:223-237.
[61] Yin Yu, Hui-Shen Shen, Hai Wang, D. 2017, Postbuckling of sandwich plates with graphene-reinforced composite face sheets in thermal environments, *Composites Part B,* 10.1016/j.compositesb.2017.09.045.
[62] Li CH, Shen Hui, Wang Hai, 2019, Thermal post-buckling of sandwich beams with functionally graded negative Poisson's ratio honeycomb core, *International Journal of Mechanical Sciences* 152: 289–297.